LAWRENCE
LIVERMORE
NATIONAL
LABORATORY

LLNL-JRNL-407973

Multi-model Estimates of Intercontinental Source-Receptor Relationships for Ozone Pollution

A. M. Fiore, F. J. Dentener, O. Wild, C. Cuvelier, M. G. Schultz, P. Hess, C. Textor, M. Schulz, R. Doherty, L. W. Horowitz, I. A. MacKenzie, M. G. Sanderson, D. T. Shindell, D. S. Stevenson, S. Szopa, R. Van Dingenen, G. Zeng, C. Atherton, D. Bergmann, I. Bey, G. Carmichael, W. J. Collins, B. N. Duncan, G. Faluvegi, G. Folberth, M. Gauss, S. Gong, D. Hauglustaine, T. Holloway, I. S. A. Isaksen, D. J. Jacob, J. E. Jonson, J. W. Kaminski, T. J. Keating, A. Lupu, E. Marmer, V. Montanaro, R. Park, G. Pitari, K. J. Pringle, J. A. Pyle, S. Schroeder, M. G. Vivanco, P. Wind, G. Wojcik, S. Wu, A. Zuber

October 21, 2008

Journal of Geophysical Research

Disclaimer

Multi-model Estimates of Intercontinental Source-Receptor Relationships for Ozone Pollution

A.M. Fiore[1], F.J. Dentener[2], O. Wild[3], C. Cuvelier[2], M.G. Schultz[4], P. Hess[5], C. Textor[6,7], M. Schulz[7], R.M. Doherty[8], L.W. Horowitz[1], I.A. MacKenzie[8], M.G. Sanderson[9], D.T. Shindell[10], D.S. Stevenson[8], S.Szopa[7], R.Van Dingenen[2], G. Zeng[11,29], C. Atherton[12], D. Bergmann[12], I.Bey[13], G. Carmichael[14], W.J. Collins[9], B.N. Duncan[15], G. Faluvegi[10], G. Folberth[13], M. Gauss[16], S. Gong[17], D. Hauglustaine[7], T. Holloway[18], I.S.A. Isaksen[16], D.J. Jacob[19], J.E. Jonson[20], J. W. Kaminski[21], T.J. Keating[22], A. Lupu[21], E. Marmer[2], V. Montanaro[23], R.J. Park[19,24], G. Pitari[23], K.J. Pringle[9,25], J.A. Pyle[11], S. Schroeder[4], M.G.Vivanco[26], P. Wind[20], G. Wojcik[27], S. Wu[19], A. Zuber[28]

1. NOAA Geophysical Fluid Dynamics Laboratory, Princeton, NJ, USA.
2. European Commission, DG-Joint Research Centre, Institute for Environment and Sustainability, Ispra, Italy.
3. Department of Environmental Science, Lancaster University, UK.
4. ICG-2, Forschungszentrum-Jülich, Germany.
5. National Center for Atmospheric Research, Boulder, CO, USA.
6. Service d'Aéronomie, CNRS/UPMC/IPSL, Paris, France.
7. Laboratoire des Sciences du Climat et de l'Environnement, CEA/CNRS/UVSQ/IPSL, Gif-sur-Yvette, France.
8. School of GeoSciences, University of Edinburgh, UK.
9. Met Office Hadley Centre, Exeter, UK.
10. NASA Goddard Institute for Space Studies and Columbia University, New York, NY, USA.
11. National Centre for Atmospheric Science, Department of Chemistry, University of Cambridge, UK.
12. Atmospheric Science Division, Lawrence Livermore National Laboratory, CA, USA.
13. EPFL, Lausanne, Switzerland.
14. Center for Global and Regional Environmental Research, University of Iowa, Iowa City, IA, USA.
15. Goddard Earth Sciences & Technology Center, UMBC, MD, USA.
16. Department of Geosciences, University of Oslo, Norway.
17. Science and Technology Branch, Environment Canada, Toronto, Canada.
18. Center for Sustainability and the Global Environment, University of Wisconsin-Madison, Madison, WI, USA.
19. Atmospheric Chemistry Modeling Group, Harvard University, Cambridge, MA, USA.
20. Norwegian Meteorological Institute, Oslo, Norway.
21. Center for Research in Earth and Space Science, York University, Canada.
22. Office of Policy Analysis and Review, Environmental Protection Agency, Washington DC, USA.
23. Dipartimento di Fisica, Universita de L'Aquila, Italy.
24. Now at Seoul National University, Korea.
25. Now at Max Planck Institute for Chemistry, Mainz, Germany.
26. CIEMAT, Madrid, Spain.

27. Northrop Grumman Corporation, VA, USA.
28. Environment Directorate General, European Commission, Brussels, Belgium.
29. Now at NIWA, Lauder, New Zealand.

Index Terms:
0368 Troposphere: constituent transport and chemistry
0478 Pollution: urban, regional and global
0345 Pollution: urban and regional
3300 ATMOSPHERIC PROCESSES
6620 Science policy

Running Title: Hemispheric Transport of Ozone Pollution

Keywords: surface ozone, intercontinental transport, methane

Abstract

Understanding the surface O_3 response over a "receptor" region to emission changes over a foreign "source" region is key to evaluating the potential gains from an international approach to abate ozone (O_3) pollution. We apply an ensemble of 21 global and hemispheric chemical transport models to estimate the spatial average surface O_3 response over East Asia (EA), Europe (EU), North America (NA) and South Asia (SA) to 20% decreases in anthropogenic emissions of the O_3 precursors, NO_x, NMVOC, and CO (individually and combined), from each of these regions. We find that the ensemble mean surface O_3 concentrations in the base case (year 2001) simulation matches available observations throughout the year over EU but overestimates them by >10 ppb during summer and early fall over the eastern U.S. and Japan. The sum of the O_3 responses to NO_x, CO, and NMVOC decreases separately is approximately equal to that from a simultaneous reduction of all precursors. We define a continental-scale "import sensitivity" as the ratio of the O_3 response to the 20% reductions in foreign versus "domestic" (*i.e.*, over the source region itself) emissions. For example, the combined reduction of emissions from the 3 foreign regions produces an ensemble spatial mean decrease of 0.6 ppb over EU (0.4 ppb from NA), less than the 0.8 ppb from the reduction of EU emissions, leading to an import sensitivity ratio of 0.7. The ensemble mean surface O_3 response to foreign emissions is largest in spring and late fall (0.7-0.9 ppb decrease in all regions from the combined precursor reductions in the 3 foreign regions), with import sensitivities ranging from 0.5 to 1.1 (responses to domestic emission reductions are 0.8-1.6 ppb). High O_3 values are much more sensitive to domestic emissions than to foreign emissions, as indicated by lower import sensitivities of 0.2 to 0.3 during July in EA, EU, and NA when O_3 levels are typically highest, and by the weaker relative response of annual incidences of daily maximum 8-hour average O_3 above 60 ppb to emission reductions in a foreign region (<10-20% of that to domestic) as compared to the annual mean response (up to 50% of that to domestic). Applying the ensemble annual mean results to changes in anthropogenic emissions from 1996 to 2002, we estimate a Northern Hemispheric increase in background surface O_3 of about 0.1 ppb yr^{-1}, at the low end of the 0.1-0.5 ppb yr^{-1} derived from observations. From an additional simulation in which

global atmospheric methane was reduced, we infer that 20% reductions in anthropogenic methane emissions from a foreign source region would yield an O_3 response in a receptor region that roughly equals that produced by combined 20% reductions of anthropogenic NO_x, NMVOC and CO emissions from the foreign source region.

1. Introduction

Reducing aerosol and ozone (O_3) levels in surface air would improve public health as exposure to these atmospheric constituents aggravates respiratory illness and may lead to premature mortality [*World Health Organization*, 2005]. Findings from numerous observational and modeling studies indicate that long-range transport of pollutants degrade air quality over remote continents [*e.g.*, *Wilkening et al.*, 2000; *Holloway et al.*, 2003; *Akimoto et al.*, 2003]. Satellite images of aerosols, particularly dust and smoke, illustrate the capacity for dust storms and biomass burning to influence tropospheric composition on a hemispheric scale [*e.g.*, *Husar et al.*, 2001]. Ground-based measurements of aerosol composition provide evidence for a foreign influence in surface air; for example, the presence of smoke from Siberian fires and dust from Asia and Africa over the United States [*e.g.*, *Prospero*, 1999; *Jaffe et al*., 2003a, 2004]. In contrast, attributing O_3 pollution to a specific source region is complicated by the interplay of processes influencing intercontinental transport (export from the source region; evolution in transit due to chemical production, chemical and depositional losses, and dilution; and mixing with surface air over the receptor region), and by a large hemispheric background and the dominance of local emissions in contributing to high-O_3 events [*e.g.*, *Derwent et al.*, 2003; *Fiore et al.*, 2003; *Goldstein et al*., 2004; *Jonson et al*., 2005]. Given the difficulty of diagnosing O_3 source-receptor (SR) relationships (*i.e*., the change in O_3 over a receptor region produced by emission changes within a source region) from observations, estimates of these relationships rely heavily on models. Here, we use an ensemble of 21 global and hemispheric chemical transport models (CTMs; Table A1) to quantify the impact of O_3 precursor emissions from four major continental-scale source regions in the Northern Hemisphere on surface O_3 in the same four "receptor" regions (Figure 1). Prior studies indicate that multi-model mean results better represent a range of observations than any individual model [*Schulz et al.*, 2006; *Stevenson et al*., 2006; *Reichler and Kim*, 2008]; the range of results across individual models provides a measure of uncertainty in our understanding as represented in the current generation of CTMs.

Tropospheric O_3 is produced via the photochemical oxidation of volatile organic compounds (VOC) and carbon monoxide (CO) in the presence of nitrogen oxides (NO_x). To date, regulations to abate surface O_3 pollution address emissions of the traditional O_3 precursors (NO_x, non-methane VOC (NMVOC) and CO) which react within hours-to-weeks to produce a "short-term" O_3 response. By altering hydroxyl radical (OH) concentrations, perturbations to emissions of these species affect the lifetime of methane (CH_4), the most abundant atmospheric VOC and a major precursor to O_3 in the remote troposphere [*Crutzen*, 1973; *Prather*, 1996; *Daniel and Solomon*, 1998; *Fuglestvedt et al*., 1999; *Derwent et al*., 2001; *Collins et al*., 2002], producing a "long-term" influence on surface O_3. This "long-term" O_3 response occurs on the methane perturbation time scale, is spatially distributed following the O_3 production from CH_4, and somewhat

offsets the O_3 response to perturbations in surface NO_x emissions, while enhancing the response to NMVOC and CO emission changes. [*Wild et al*, 2001; *West et al*., 2007]. Anthropogenic CH_4 emissions have also been shown to contribute directly to O_3 in surface air [*Fiore et al*., 2002a; *Dentener et al.*, 2005; *West et al.*, 2007; *Fiore et al*., 2008]. The contributions to surface O_3 over a receptor region both from CH_4 and from the foreign emissions of the traditional O_3 precursors are generally considered to be part of the "background" O_3 level (along with natural precursor emissions), and have not generally been considered in air pollution mitigation strategies.

Analysis of observations at northern mid-latitudes indicate that background O_3 has been increasing in recent years, although estimates vary, with some revealing little change [*e.g., Vingarzan*, 2004; *TF HTAP*, 2007; *Oltmans et al.*, 2006; *Derwent et al*., 2007; *Schultz et al*., 2007]. Several modeling studies suggest that projected increases in emissions around the globe will enhance hemispheric background O_3 in the coming decades, potentially offsetting efforts to improve regional air quality via controls on domestic precursor emissions [e.g. *Jacob et al*., 1999; *Yienger et al.*, 2000; *Collins et al*., 2000; *Fiore et al.* 2002a; *Dentener et al*., 2005; *Derwent et al*., 2006; *Szopa et al.*, 2006; *Ellingsen et al*., 2008]. Efforts to improve air quality typically focus on controlling local and regional sources. In nations where O_3 precursors have been regulated for decades, the combination of increasing hemispheric background levels and mounting control costs could make pursuing international cooperation an attractive option [*Keating et al*., 2004; *Bergin et al*., 2005; *Solberg et al*., 2005]. An international approach to air quality management will require a strong scientific understanding of the SR relationships between continents and nations.

Under the United Nations Economic Commission for Europe (UNECE) Convention on Long Range Transboundary Air Pollution (CLRTAP), the Task Force on Hemispheric Transport of Air Pollution (TF HTAP; www.htap.org) was established to advance the understanding of hemispheric transport of air pollutants in the Northern Hemisphere. A major TF HTAP activity is to coordinate a multi-model effort to quantify and estimate uncertainties in intercontinental SR relationships for O_3, aerosols, mercury, and persistent organic pollutants. Companion manuscripts investigate NO_y deposition [*Sanderson et al*., 2008], transport with idealized tracers [*Schultz et al*, 2008, in prep], the Arctic as a receptor region [*Shindell et al*, 2008], and aerosols [*Schulz et al*, 2008, in prep].

Prior estimates for intercontinental SR relationships differ by factors of about 2 to 6 for a given SR pair among source regions at northern mid-latitudes [*TF HTAP*, 2007 and references therein]. Comparison among prior studies, however, is limited by methodological differences, including definitions of source and receptor regions, reported metrics, period of analysis, and SR calculation method [*TF HTAP*, 2007]. Observational analyses have compared concentration differences in air masses originating from a source region versus a background value [*e.g. Huntrieser et al*., 2005; *Derwent et al*., 1998; *Jaffe et al*., 2003b]. A suite of methods for source attribution have been applied in models, including marking tracers by region of O_3 production [*e.g. Jaeglé et al*., 2003; *Derwent et al*., 2004], labeling by the regional NO_x source contributing to O_3 production [*Hess and Lamarque*, 2007], and perturbing regional emissions [*e.g. Jacob et al.*, 1999; *Yienger et al.*, 2000; *Wild and Akimoto*, 2001; *Fiore et al.*, 2002b, *Auvray and Bey*, 2005].

The approach adopted here builds upon these previous studies by applying a consistent experimental design across multiple models to provide an estimate of SR relationships throughout the year. Specifically, we investigate the changes in surface O_3 resulting from fixed percentage reductions in anthropogenic O_3 precursors (NO_x, CO, CH_4, and NMVOC). We first describe the modeling framework (Section 2) and evaluate the base case simulations with observations of surface O_3 (Section 3). Our analysis focuses on two continental-scale SR metrics: (1) the response, defined as the spatially averaged absolute change in O_3 concentrations over a receptor region due to emission changes in a source region, and (2) the "import sensitivity", defined as the ratio of the sum of the spatially averaged changes in surface O_3 in a continental receptor region resulting from perturbations to precursor emissions in the three foreign source regions to the surface O_3 change resulting from the same percentage perturbation to domestic emissions (*i.e.*, emissions within the continental receptor region; Section 4). We then examine the response of surface O_3 to changes in CH_4 levels (Section 5). In an effort to relate our results more directly to statistics commonly employed in air quality management, we also analyze the response of a threshold indicator of air quality to emission changes (Section 6). Finally, we apply our SR relationships to evaluate the role of reported trends in Asian emissions on trends in northern mid-latitude surface O_3 observed in recent decades (Section 7).

2. Model Simulations and Emissions

Simulations designed to estimate intercontinental source-receptor (SR) relationships for O_3 were conducted in 21 chemical transport models (CTMs) (Table A1). Initial results were reported by *TF HTAP* [2007]; we expand here upon that analysis. Most models were driven by meteorological fields from one of several reanalysis centers (either prescribed directly or via linear relaxation) for the year 2001, although four models were general circulation models with meteorology generated based on observed sea surface temperatures for 2001 (Table A1). Model horizontal resolution ranged from 5° x 5° to 1° x 1°, with resolutions of 3º x 3º or finer in about half of the models, similar to the ACCENT/AR4 intercomparison [*Dentener et al*, 2006; *Stevenson et al*. 2006]. CH_4 concentrations were set to a uniform mixing ratio of 1760 ppb and modeling groups were requested to use their best estimate of O_3 precursor emissions for the year 2001 (Tables A2 and A3); the use of different emission inventories contributes to the inter-model differences in our results.

We consider four major source regions at northern mid-latitudes (Figure 1): East Asia (EA), Europe and northern Africa (EU), North America (NA), and South Asia (SA). The EU and EA regions span roughly equivalent areas (2.1×10^7 and 2.3×10^7 km^2), with NA somewhat larger (2.6×10^7 km^2) and nearly twice the area of SA (1.5×10^7 km^2). Anthropogenic emissions of NO_x and NMVOC from EU, NA, and EA are similar in the model ensemble mean (μ) to within ~30% (Table 1; Tables A2 and A3 list the emissions used by individual models). The standard deviation (σ) indicates the diversity of the emission inventories used in the models, with the smallest relative inter-model spread for anthropogenic NO_x emissions in EU and NA (σ/μ <10%) and the largest spread for anthropogenic NMVOC from EU (σ/μ = 58%). A comparison of the model ensemble mean anthropogenic and total (which also includes biomass burning and biogenic

contributions) emissions in Table 1 shows a dominant contribution (>70%) from anthropogenic NO_x and CO in all regions considered. For the ensemble mean NMVOC emissions, biogenic emissions dominate in all regions except for EU where anthropogenic and biogenic contributions are approximately equal.

Relative to SR1, we conduct 16 sensitivity simulations in which anthropogenic emissions of the traditional O_3 precursors (NO_x, NMVOC, and CO) are reduced by 20% individually (simulations SR3, SR4, and SR5, respectively) and jointly along with aerosols ("ALL"; simulation SR6) within each of the four source regions in Figure 1. These simulations are labeled hereafter according to the respective emission scenario and the region in which emission reductions were applied (*e.g.*, SR3EA identifies the simulations with 20% reductions of anthropogenic NO_x emissions within East Asia). An additional sensitivity simulation was conducted in which the CH_4 mixing ratio was decreased by 20% (to 1408 ppb) and other O_3 precursor emissions were not changed (SR2). The results from this simulation are interpreted in Section 5.3 in an effort to compare more directly the probable ozone response from regional reductions of anthropogenic CH_4 emissions to that from the regional reductions in emissions of other O_3 precursors simulated in the SR3, SR4, SR5 and SR6 experiments. All simulations were conducted for a full year, following a minimum of six months initialization, a sufficient time for the simulated trace gas concentrations to fully respond to the imposed emission or concentration perturbations given our use of uniform CH_4 mixing ratios; responses on longer time scales are diagnosed in Section 5.2. The number of models participating in each of the sensitivity simulations ranges from 13 to 18 (Table A4).

The perturbation magnitude of 20% reflects a compromise between producing a clear signal in the O_3 simulations and applying a sufficiently small perturbation to allow the results to be scaled linearly to different size perturbations. Under the ACCENT/AR4 Experiment 2, *Stevenson et al.* [2006] found a broadly linear relationship between the 26-model mean tropospheric O_3 burden and global NO_x emissions within the ±50% range of present day emissions considered in that study, although those simulations did not exclusively change NO_x emissions. The scalability of our results to perturbations of other magnitudes is examined further for NO_x in Section 4.2, and has been shown to hold for the O_3 response to changes in CH_4 over the range of present-day anthropogenic emissions [*Fiore et al*., 2008]. We approximate the O_3 response to simultaneous reductions in multiple regions as the sum of the O_3 responses to the individual regional reductions. Companion work suggests that such linearity should hold for the NMVOC and CO emission reductions but that this approach may underestimate the O_3 response to NO_x emission reductions imposed simultaneously in multiple regions [*Wu et al.*, in prep; see also Section 4.2].

3. Model Evaluation with Surface Observations

We first calculate the spatial average (area-weighted) surface O_3 mixing ratios over each of the four regions in Figure 1, using the values from the lowest level grid boxes in each model. In the base simulation (SR1), the 21-model annual spatial mean surface O_3 mixing ratios and their standard deviations (across models) over the four continental source regions in Figure 1 are similar: 36.2±3.9 ppb for NA, 37.8±4.5 for EU, 35.8±3.0 for EA, and 39.6±4.0 for SA. The largest ensemble mean peak-to-peak

amplitude (difference between the maximum and minimum months) occurs in EU (19.8±5.9 ppb), possibly reflecting NO_x titration in the stronger wintertime boundary layer compared to the other regions (10.4±2.6 for NA; 12.7±3.2 for EA, and 14.8±6.0 for SA).

A major challenge to assessing model skill at representing the O_3 response to foreign (or domestic) emission changes arises from the difficulty of directly observing these relationships (particularly in surface air). Testing the models with simultaneous measurements of O_3 and related species is preferable [*e.g. Sillman*, 1999]; such observations are mainly limited to intensive field campaigns, which are the focus of an ongoing TF HTAP multi-model study. A companion study will evaluate the models with the ozonesonde network [*Jonson et al*., in prep]. Many of the models in our study have been compared with ozone observations for the year 2000 as part of the ACCENT/AR4 Experiment 2 study [e.g., *Dentener et al*., 2006; *Stevenson et al*., 2006; *Ellingsen et al*., 2008]. Annual mean surface O_3 concentrations were within 5 ppb of the measurements in the United States, China, and Central Europe (out of total observed values of 40-50 ppb) [*Dentener et al*., 2006]. Overestimates of 10-15 ppb (out of total observed values of 20-40 ppb) were found in Africa, India, and the Mediterranean, for reasons not yet understood [*Dentener et al*., 2006; *Ellingsen et al*., 2008].

Due to limited availability of surface O_3 measurements over India, China, and Africa, we focus here on the widespread observational networks in the United States, Europe, and Japan (Figure 2). While spatially-averaged concentrations over the regions in Figure 2 often differ by more than 15 ppb in the individual models, the model ensemble mean generally captures the observed seasonal cycle and is close to the observed regional mean. A wide range of simulated tropospheric O_3 budgets has been documented in the literature, attributed in part to factors that are likely to contribute to inter-model variability in simulated surface O_3 concentrations, such as differences in surface emissions of NO_x and isoprene, as well as in model treatment of dry deposition, heterogeneous chemistry and the organic nitrates from isoprene [*Stevenson et al*., 2006; *Wu et al*., 2006; *Wild*, 2007; *Ellingsen et al*., 2008].

We separate the observational sites at low elevations from those at higher altitudes in Figure 2 since high altitude sites more frequently sample free tropospheric air and thus are better suited to detecting hemispheric pollutant transport (which occurs most efficiently in the free troposphere) prior to mixing with local pollutant signals in the planetary boundary layer [*Cooper and Moody*, 2000; *Trickl et al*., 2003; *Weiss-Penzias et al*., 2006]. All models are sampled at the lowest level (surface) within the grid cell corresponding to each site location (including for high-altitude sites). At the high altitude sites (Figures 2c and 2h), the models tend to underestimate O_3 concentrations. Steep topographic gradients that are averaged out within one model grid cell, particularly over Europe, may be responsible if the measurements are more representative of the free troposphere than the models' surface layer (where O_3 deposition leads to lower concentrations); additionally, the coarse resolution of global models cannot represent local orographically-driven flows or sharp gradients in mixing depths.

The model ensemble mean and median exhibit little bias at low-altitude European sites and capture the seasonal cycle (Figures 2a and 2b), an apparent improvement over the underestimate in summer months found by *Ellingsen et al*. [2008]. In contrast, the multi-model mean overestimates the observed summertime surface O_3 concentrations

over Japan (bias of 12 ppb; Figure 2i) and in the eastern U.S. (bias greater than 14 ppb in July in Figures 2d, 2f and 2g). The observed summer minimum in O_3 over Japan occurs during the wet season of the Asian monsoon. Results from the MICS-Asia regional model intercomparison suggest that the positive model bias in this season may stem from inadequate representation of southwesterly inflow of clean marine air [*Han et al*., 2008; *Holloway et al*., 2008]. Examination of inter-model differences in this region with the TF HTAP idealized tracer transport simulations [*Schultz et al*., in prep] should provide further insights into the source of this problem.

Ellingsen et al. [2008] also found an overestimate of surface O_3 levels in July through September for the year 2000 over the Great Lakes and in June through September over the Southeastern United States. In July and August, however, the ensemble median value fell within the standard deviation of the observations. We find that the observed July and August average O_3 decreased by 10 ppb from 2000 to 2001; the larger model error shown in Figure 2 than found by *Ellingsen et al*. [2008] suggests that the model ensemble mean does not capture the observed interannual variability over the eastern United States, although our use of different emission inventories than those used in *Ellingsen et al.* [2008] may also play a role. The bias is particularly large over the southeastern U.S. where uncertainties in isoprene-NO_x-O_3 chemistry may contribute; smaller biogenic NMVOC emissions over Europe (difference between total and anthropogenic NMVOC in Table 1) would lessen the impact of any problems in this chemistry on surface O_3 concentrations there. The bias is not driven by nighttime processes since restricting our comparison to afternoon hours does not yield any improvement (Figure A1). The sensitivity of surface O_3 over all regions to the 3 foreign source regions is strongest in spring and late autumn (Section 4.1) when the model ensemble mean matches the observed values in all regions. We further examine the potential influence of the bias on the predicted source-receptor relationships during summer in Section 4.3.

4. Source-Receptor Relationships for NO_x, NMVOC and CO

4.1 Model ensemble mean results

Figure 3 (and Table A4) shows the annual average surface O_3 response in the receptor regions to 20% regional reductions of anthropogenic NO_x, CO, NMVOC emissions, individually and all together ("ALL"), as well as the sum of the responses to emission perturbations in the 3 foreign source regions (for a discussion of linearity see Section 4.2). In most receptor regions, O_3 responds strongly to NO_x, followed by NMVOC and CO, respectively. An exception occurs for EU emissions where the model ensemble O_3 response to NMVOC is comparable to that from NO_x. The relative dominance of NO_x diminishes when the long-term feedback through CH_4 is taken into account (Section 5.2). For all SR pairs, domestic emission reductions are most effective at reducing surface O_3. Surface O_3 also decreases when emissions are reduced in a foreign source region, sometimes by >10% of the decrease attained from the same percentage reduction of domestic emissions (Figure 3 and bold entries in Table A4). In some cases, annual mean responses to foreign emissions are as large as ~50% of the response to domestic emissions, as occurs for NA NO_x, CO, and ALL on surface O_3 in EU; for EU NMVOC on surface O_3 in SA; and for EA CO on surface O_3 in NA and EU.

We next examine seasonality in these SR relationships, beginning with the seasonal cycle in the O_3 response to domestic emission reductions (filled circles in Figure 4). Over all regions, the domestic response to the 20% decrease in CO emissions (~0.1 ppb) varies little during the year while the response to NO_x exhibits the strongest seasonality (max of >1 ppb). Over EU, NO_x reductions increase the model ensemble mean O_3 from November to March. The surface O_3 decrease from NMVOC emission reductions is largest in boreal winter (up to ~0.5 ppb over EU, though seasonality is weak), when biogenic emissions, radiation, and humidity are at their seasonal minimum and O_3 production is more sensitive to anthropogenic NMVOC [*Jacob et al.*, 1995]. The seasonality of the domestic response to ALL is largely driven by NO_x, peaking in summer for NA, EU, and EA, and in October through March for SA. The different seasonality over SA reflects the influence of the Asian monsoon (wet season during boreal summer).

We find that intercontinental transport contributes most to surface O_3 concentrations at northern mid-latitudes during boreal spring and fall (filled circles in Figure 5), reflecting a combination of more frequent storm tracks that enhance ventilation of the continental boundary layer, more efficient transport in stronger mid-latitude westerly flow in the free troposphere, and a longer O_3 lifetime allowing for a longer transport distance than in summer when O_3 production and loss (both chemical and depositional) are largest [*Wang et al.*, 1998; *Jaffe et al.*, 1999; *Yienger et al.*, 2000; *Bey et al.*, 2001;*Wild and Akimoto*, 2001; *Stohl et al.*, 2002; *Liu et al.*, 2003; *Weiss-Penzias et al.*, 2004; *Wild et al.*, 2004; *Liu et al.*, 2005; *Holzer et al.*, 2005; *Holloway et al.*, 2008]. Over all regions, the summed responses to 20% decreases in anthropogenic NO_x emissions from all 3 foreign regions are largest in boreal spring and fall to early winter (up to ~0.4 ppb); the response to NMVOC emissions in the 3 foreign regions is largest in winter through early spring (0.2-0.4 ppb). Over NA, the model ensemble average O_3 response to NO_x and NMVOC emissions in the 3 foreign regions are similar (~0.3 ppb) in winter, spring and summer, although this result varies across models (Section 4.3). The 20% reductions of CO emissions in the 3 foreign regions have little influence (<0.2 ppb) on surface O_3 over the receptor regions, but this influence increases when the long-term feedback via CH_4 is included (Section 5.2).

In Figure 6, we decompose the foreign impact in the "ALL" simulations into the contributions from each of the 3 foreign source regions. For the NA receptor region, EA and EU contribute similarly from April through November. NA contributes most strongly to EU throughout the year, reflecting its upwind proximity. The SA source region exerts a minor influence throughout the year on surface O_3 over NA and EU (always less than 0.1 ppb to surface O_3), as SA pollution is typically funneled away from the northern mid-latitude westerlies (the dominant transport pathway to those regions) [*e.g., Li et al.*, 2001; *Lelieveld et al.*, 2002a; *TF HTAP* 2007], and tends to remain isolated from mid-latitude air [*Bowman and Carrie*, 2002; *Hess*, 2005]. Over EA, emissions from the 3 foreign source regions induce a similar response in surface O_3 during summer, with stronger sensitivity to emissions in EU (followed by NA) during spring, and to NA (followed by EU) in winter. Over SA, the surface O_3 response is largest when emissions are reduced in EU, except for the November peak which is driven by emissions from EA. For part of the year, surface O_3 over the receptor regions is similarly influenced by at least 2 foreign source regions, except for EU which is always influenced most by NA.

In order to compare the surface O_3 response to emission reductions in the 3 foreign regions versus the domestic region, we define a regional "import sensitivity" (IS_r):

$$IS_r = \left(\sum_{f=1}^{3} \Delta O3_{fr} \right) / \Delta O3_{rr}$$

where IS_r represents the import sensitivity for receptor region *r*; $\Delta O3_{fr}$ represents the model ensemble mean change in surface O_3, spatially averaged over the receptor region *r*, produced by a 20% decrease in anthropogenic emissions over the foreign source region (*f*); $\Delta O3_{rr}$ is the change in surface O_3 resulting from the 20% reduction of anthropogenic emissions within the domestic source region. The larger the value of the import sensitivity, the greater the relative influence of emissions from the 3 foreign regions. Note that the import sensitivity neglects the influence of foreign emissions in regions not considered here, and is unlikely to be representative of the relative importance of foreign versus domestic emission changes in urban airsheds not resolved by global models. Nevertheless, this metric enables us to gauge the large-scale O_3 responses to foreign versus domestic emission changes, and how their relative importance varies by region and season.

The annual mean IS_r ranges from approximately 0.3 (NA and SA) to 0.7 (EU) for NO_x alone; 0.4 (EU) to 1.1 (SA) for NMVOC alone; and 0.5 (NA and SA) to 0.7 (EU) for the combined reductions in all O_3 precursors. The IS_r for CO ranges from approximately 0.8 (EA) to 1.2 (EU), reflecting the longer CO lifetime and the correspondingly smaller influence from domestic sources. Monthly mean IS_r estimates from the ALL simulations are shown in Figure 7. Over EA, NA, and EU, IS_r exceeds 1 during boreal winter (also in early spring and late fall over EU) when the O_3 response to domestic emissions is small (Figure 4). Even in summer, when domestic O_3 production peaks, IS_r is 0.2-0.3 over these regions. During the month with the largest absolute surface O_3 response to ALL emission reductions in the 3 foreign regions (Figure 6), IS_{NA}= 0.6 (April), IS_{EU}=0.7 (April), and IS_{EA}=1.1 (March). The IS_{SA} for ALL varies little during the year (Figure 7) and is ~0.5 in November and during the broad secondary peak of influence from the 3 foreign regions from January through April (Figure 6). We conclude that the O_3 response to emissions in the 3 foreign regions is not negligible when compared to the response to domestic emissions, and is particularly strong in spring and fall at northern mid-latitudes.

4.2 Applicability of results to other emission perturbations

Evaluating whether the O_3 response to multi-component emission reductions is equivalent to the sum of the responses to single component emission reductions is critical for determining the applicability of our results to other combinations of precursor emission reductions. In order to assess the additivity of our simulations, we construct the ratio of the sum of the O_3 response to 20% reductions in emissions of the individual precursors NO_x, NMVOC, and CO, *i.e.*, (SR3-SR1)+(SR4-SR1)+(SR5-SR1) to the O_3 response in the simulation where all precursors (along with aerosols) were reduced simultaneously (SR6-SR1). With one exception, models including reductions of aerosols and aerosol precursors in SR6 indicate that the sum of the responses to single component emission reductions exceeds that to multi-component perturbations, by as much as 50% for some SR pairs (Table A5 and Figure A3). The degree of additivity varies by region within individual models (Figure A3). In Figure 8, we restrict our analysis to those

models without aerosol changes in SR6, and find that the summed surface O_3 responses to single-component emission reductions are approximately equivalent to those from multi-component reductions for emission changes in the domestic and the 3 foreign source regions combined. We conclude that combined reductions in emissions of aerosols and O_3 precursors dampen the O_3 response relative to that produced by emission reductions of the O_3 precursors alone. Only two out of six of these models include feedbacks of aerosol changes on photolysis rates (Table A5), so this damping effect must operate primarily through chemical interactions in the models, for example by reducing aerosol uptake of O_3 precursors.

If we wish to apply the responses diagnosed in Section 4.1 more broadly, we need to determine if the O_3 response is sufficiently linear to yield accurate results when scaling to emission perturbations of other magnitudes. To address this point, additional simulations with varying sized perturbations to EU anthropogenic NO_x emissions were conducted in the FRSGC/UCI model [*Wild et al.*, 2003]. The FRSGC/UCI model tends to produce a larger surface O_3 response to NO_x than the model ensemble mean, but is not an outlier in any month, so we expect these results to apply generally to our model ensemble. Figure 9 shows the response of surface O_3 over EU and NA. The EU source region was chosen as it exhibits the most non-linear response of all regions (*e.g.*, reversing sign with season in Figure 4). The response over the source region (EU) deviates more from that obtained by a linear scaling of the response in the 20% perturbation simulation than over a remote receptor region (NA). For example, the summertime response over the EU remains linear only for perturbations within 20%, whereas it is fairly linear well beyond perturbations of 50% over NA. The response is most linear in summer over the foreign receptor region. A companion manuscript [*Wu et al.*, in preparation] expands this analysis by incorporating simulations from other models, perturbations to other O_3 precursor emissions, and in other source regions.

4.3 *Robustness of results as measured by inter-model differences*

We first examine whether the surface O_3 bias versus observations in the individual models over the eastern United States (Section 3) manifests as a larger response, for example, of EU surface O_3 to the reductions in NA emissions. We find little correlation between the bias and the simulated SR relationships ($r^2<0.1$ for the EU response to NA emission changes in July). The source of the bias, however, requires further investigation to increase confidence in the estimates for summertime SR relationships for the NA and EA regions.

We next interpret the model range of O_3 responses to emission changes as a measure of the combined uncertainty from differences in the emission inventories and the representations of transport and photochemical processes in the individual models. The model spread (measured by the relative standard deviation, σ/μ) associated with the O_3 response to decreases in NMVOC emissions is often larger than that due to reductions in either NO_x or CO emissions (Table A4), and probably reflects the larger uncertainty associated with the NMVOC inventories and the incorporation of the individual NMVOC species into the model chemical mechanisms (Table 1). For example, Figure 10 shows that the magnitude of the surface O_3 response over NA to decreases in EU anthropogenic NMVOC emissions in the individual models correlates ($r^2 = 0.50$) with the anthropogenic EU NMVOC emission total, which varies by nearly a factor of 10. Although Figure 5

suggests that surface O_3 over NA has a similar sensitivity to emissions of NO_x and NMVOC in the 3 foreign regions, this result varies across the models (not shown). Better constraints on the total NMVOC emissions and their partitioning into NMVOC species with different reactivity should help to reduce the associated uncertainty in the O_3 sensitivity.

For each region, we assess the robustness of the SR relationships in Figure 6 across the 15 individual models. We focus here on the springtime (March, April and May) response to the combined emissions reductions (*i.e.*, SR6-SR1; Figure A2). The rankings for the EU receptor region are most robust, with NA>EA>SA in all models. All models also indicate that springtime O_3 over EA, EU, and NA is less sensitive to emissions from SA versus the other 3 foreign regions. The model spread in the response of NA surface O_3 to emission reductions in EU versus EA in spring indicates more uncertainty, with 10 models predicting equivalent responses (to within 20%), but in 4 models the response to EA emissions is 30-55% greater than that to EU emissions. Over EA, where the winds are northwesterly during spring, the O_3 response to emission changes in EU and NA exceeds that to SA (by a factor of 1.6-3 for EU in 12 models, and 1.5-2 for NA in 9 models). Over SA, the O_3 response to emission changes rank as EU>NA>EA in 9 of 15 models for spring. Future work should investigate why some models respond differently from the majority, and the relative roles of emissions, transport, and chemistry in contributing to these differences. Priority should be placed on identifying observation-based constraints that can be used to select those models that most accurately represent the key processes contributing to hemispheric ozone transport.

4.4 Comparison with prior estimates of intercontinental source-receptor relationships

In Figure 11, we compare our results for the NA, EU, and EA regions with the studies referenced in *TF HTAP* [2007] that report annual and seasonal mean SR relationships, supplemented by recent analyses by *Lin et al.* [2008], *Duncan et al.* [2008], and *Holloway et al.* [2008]. While the range across previous studies reflects a variety of regional definitions, reported metrics, meteorological years, and methods for source attribution, the consistent modeling approach adopted here restricts the range across our model results to differences in emissions, chemistry, transport, and resolution (both horizontal and vertical). Information regarding import to or export from the SA region is limited; our results in Figure 5 for SA are consistent with those of *Kuhnikrishnan et al.* [2006] in showing an autumn peak, but in contrast to that study, we find that the response of SA surface O_3 to EA NO_x emissions is larger in winter than in summer.

For previous studies in which the O_3 response was examined for emission perturbations smaller than 100%, we scale the reported results linearly to estimate the total contribution from foreign anthropogenic emissions. To compare our model results with prior studies, we scale our responses diagnosed for 20% emission decreases to 100% by using 5*(SR1-SR6) to estimate the total contribution of anthropogenic NO_x+NMVOC+CO emissions in a foreign source region to surface O_3 in a receptor region. Figure 10 implies that a linear scaling of our 20% reductions in anthropogenic NO_x emissions will yield a smaller response than in a simulation where emissions are set to zero. The response to the combined NO_x+NMVOC+CO emission reductions should deviate less from linearity due to competing effects on OH from NO_x versus NMVOC+CO but this assumption needs further investigation. The range in annual mean

SR relationships for the EU and EA receptor regions across our model ensemble narrows considerably from the estimates in the literature, with the model ensemble response in Figure 11 smaller than most prior estimates for spring and summer. Our study provides a comprehensive view of the seasonality of SR relationships and a previously unavailable quantitative measure of inter-model spread which may indicate uncertainty in these relationships.

5. Contribution from CH_4 to the Long-term Response of O_3

5.1 Surface O_3 response to CH_4 concentrations

The ensemble annual mean surface O_3 response to a 20% decrease in global CH_4 concentrations is 1.1-1.3 ppb averaged over the receptor regions, largest in SA and EU, followed by NA and EA (Table A4). The O_3 responses in the individual models, however, differ by ~1 ppb (ranging from 0.7 to1.6 ppb over EA; 0.8 to 1.8 over EU; 0.8 to 1.7 over NA; 0.9 to1.8 over SA). This range likely reflects model differences in OH and NO_x distributions [*e.g., Fiore et al*., 2008]. Since the O_3 response to CH_4 is approximately linear over the range of present-day anthropogenic emissions [*Fiore et al*., 2008], we can scale the ensemble mean responses in Table A4 from 20% to 100% to estimate that CH_4 presently contributes 5.5-6.5 ppb to surface O_3 in the receptor regions, consistent with the multi-model estimate of *Prather et al* [2001] that anthropogenic CH_4 (~60% of the global total) contributes 4 ppb to surface O_3.

The stronger O_3 response to CH_4 over SA is consistent with its tropical location where OH is abundant and the temperature-sensitive CH_4-OH reaction proceeds faster [*e.g., Spivakovsky et al*., 2000]. One might then expect that EU, situated at more northerly latitudes than the other regions, would exhibit the weakest response of surface O_3 to CH_4. Instead, the response is nearly as strong as that found in SA, and stronger than the responses in NA and EA. The largest peak-to-peak amplitude of the O_3 response to CH_4 occurs in EU, followed by SA, NA, and EA (Figure A4). The O_3 response to CH_4 over EU is largest during summer, possibly reflecting a combination of the stronger seasonality in O_3 production in this northern region and stronger CH_4-sensitivity arising from smaller biogenic (high reactivity) VOC emissions than in the other regions. The seasonal amplitude of the EU O_3 response to CH_4 in the individual models is indeed somewhat correlated with the ratio of EU anthropogenic to total NMVOC emissions ($r = 0.7$ for 15 models).

5.2 Long-term O_3 response to NO_x, CO, and NMVOC emissions reductions

Perturbations to NO_x, CO, and NMVOC emissions influence the oxidizing capacity of the atmosphere (OH), which can change the CH_4 lifetime and thereby contribute a "long-term" change in tropospheric O_3 on the decadal time scale of the CH_4 perturbation lifetime [*e.g. Prather,* 1996; *Daniel and Solomon*, 1998; *Fuglestvedt et al*., 1999; *Wild and Prather*, 2000; *Derwent et al*., 2001; *Wild et al.*, 2001; *Collins et al*., 2002; *Stevenson et al.*, 2004]. Using the method described below, *West et al*. [2007] previously found that the long-term impacts of 20% decreases in global anthropogenic emissions on population-weighted average surface O_3 at northern mid-latitudes enhanced the short-term response by 16-21% for CO, and decreased it by 6-14% for NO_x, with little long-term influence from NMVOC. This long-term impact on surface O_3 exhibits the

spatial distribution of the surface O_3 response to changes in CH_4, which we obtain here from the difference in O_3 between the SR2 and SR1 simulations for each model (Section 5.1). By setting atmospheric CH_4 to a uniform, fixed value of 1760 ppb, the SR3 through SR6 simulations neglect the feedback on CH_4 from the changes in OH induced by the 20% decreases in regional anthropogenic NO_x, NMVOC, and CO emissions. In order to account for this feedback, we first estimate what the steady-state CH_4 concentration change would be in a simulation in which CH_4 concentrations were allowed to respond to OH changes, but with CH_4 emissions held equal to those implied by the 1760 ppb atmospheric abundance in SR1. The treatment of CH_4 as a uniform, fixed value should not introduce any error in the estimated O_3 response to changes in CH_4 since the spatial distribution of the O_3 response to CH_4 has been shown to be identical (spatial correlation of r = 1.0) in a full transient CH_4 simulation (*i.e.*, with CH_4 varying spatially) and in a simulation with CH_4 set to a globally uniform, fixed value [*Fiore et al*., 2008].

We apply the formulation of *West et al*. [2007] to estimate the CH_4 abundance that would result from the changes in the other O_3 precursor emissions:

$$[CH_4]_{SRNxx} = [CH_4]_{SR1} * (\tau_{SRNxx}/ \tau_{SR1})^F$$

where SRN represents SR3 through SR6; xx is the 2-letter regional abbreviation in Figure 1; τ_{SR1} is the total atmospheric CH_4 lifetime (assuming CH_4 losses to soils and the stratosphere with lifetimes of 160 and 120 years [*Prather et al.*, 2001], respectively). in the base simulation; τ_{SRNxx} is the CH_4 lifetime in the perturbation simulation; and F is defined as the ratio of the atmospheric response (perturbation) time to the global atmospheric lifetime (see below). Table 2 lists the subset of models that archived the CH_4 loss rates required to determine τ_{SR1}, τ_{SRNxx}, and F. The model ensemble mean τ_{SR1} = 8.55 ± 1.6 is within 2% of the 26-model mean of 8.67 ± 1.32 reported by *Stevenson et al.* [2006], and the ensemble mean methane lifetime against loss by tropospheric OH of 10.2 ± 1.7 agrees well with observationally-derived (from methyl chloroform) estimates of $10.2^{+0.9}_{-0.7}$ [*Prinn et al.*, 2005]. From the SR1 and SR2 simulations, we calculate F following *Wild and Prather* [2000]:

$$F = 1/(1-s)$$
$$s = (\ln(\tau_{SR2})- \ln(\tau_{SR1}))/(\ln(B_{SR2})-\ln(B_{SR1}))$$

where B is the total atmospheric CH_4 burden. F describes the response of the atmospheric CH_4 abundance to a change in CH_4 emissions. In the case of a small perturbation, F is approximately the ratio of the relative change in CH_4 concentrations to an imposed emission change. For example, the model ensemble mean F of 1.33 (Table 2) implies that a 1% increase in CH_4 emissions would ultimately yield a 1.33% increase in CH_4 concentrations. The multi-model mean F is at the low end of the reported range of 1.33-1.45 range (and within 10% of the recommended value of 1.4) by *Prather et al*. [2001].

Following *Naik et al*. [2005] and *West et al*. [2007], we estimate the long-term impact on O_3 by scaling linearly the change in surface O_3 in the CH_4 perturbation simulation (SR2-SR1) for each model grid cell by the ratio of the estimated changes in CH_4 from SR1 to SRNxx versus SR2:

ΔO_3 (SRNxx – SR1) = [ΔCH_4 (SRNxx – SR1)/ ΔCH_4 (SR2-SR1)] * ΔO_3 (SR2-SR1)

For each model, we then calculate the domain average "long-term" O_3 response for each region in Figure 1 and add this ΔO_3 to the short-term O_3 response (averaged over each region) diagnosed directly from SRNxx-SR1.

Including the long-term feedback through CH_4 has little impact on the model ensemble mean domestic response (solid vs. dotted lines in Figure 4). In contrast, a larger percentage change occurs for the O_3 response to emissions in foreign regions since the O_3 response to changes in CH_4 (SR2-SR1) is relatively uniform globally. Figure 5 shows that the long-term contribution partially offsets the estimated O_3 decrease from NO_x emission reductions within the 3 foreign regions, since the net global effect of decreasing surface NO_x emissions is to lower OH, causing the CH_4 abundance to rise, thereby enhancing the CH_4 contribution to surface O_3. During the month of maximum contribution from the 3 foreign regions (April for NA, EU, and EA and November for SA), the long-term effect reduces the short-term O_3 decrease by ~15-20%. During the same months, the short-term O_3 responses to the 20% reductions in CO and NMVOC emissions from the 3 foreign regions are augmented by 30-40% and ~10%, respectively, since decreasing CO or NMVOC increases OH. These results are qualitatively consistent with those of *West et al*. [2007]. Over NA and EU during summer, the opposing influences of the long-term feedback from NO_x and CO result in the total impact of the CO emission reductions exceeding that from NO_x (or NMVOC). As there is little seasonality in the O_3 response to CH_4 (SR2-SR1), the seasonal cycle of the total O_3 response is mainly driven by the short-term response to the changes in NO_x, CO, and NMVOC emissions (Figure 6).

In the case of the simultaneous reductions in NO_x, NMVOC, and CO emissions from all 3 foreign regions, the long-term feedback is minimal (always less than 3% for all months and regions in Figure 5). The balancing effect of simultaneous changes of NO_x, CO, and NMVOC has been noted before in the context of the remarkable stability of OH concentrations from the pre-industrial to the present-day atmosphere [*Wang and Jacob*, 1998; *Lelieveld et al*., 2002b]. Since anthropogenic sources of NO_x, CO, and NMVOC differ, however, equivalent percentage reductions would not necessarily be applied to all precursors together, in which case the long-term effect should be considered.

5.*3 Inferring the O_3 response to regional reductions in anthropogenic CH_4 emissions*

The results from the simulation in which the global CH_4 abundance was decreased uniformly by 20% are not directly comparable with those from the 20% regional reductions of the other O_3 precursors. In this section we attempt such a comparison by approximating the surface O_3 response that would result from 20% reductions of CH_4 anthropogenic emissions in the source regions.

We first use ensemble mean results to estimate the anthropogenic CH_4 emission decrease that would produce the 20% reduction in global concentrations applied in the SR2 simulation. Applying the model ensemble mean feedback factor (F) of 1.33 from Table 2 (Section 5.1) to account for the feedback of CH_4 on its own lifetime, we derive that the 20% decrease in CH_4 abundance corresponds to a 15.4% decrease in total global

CH_4 emissions. Assuming that anthropogenic CH_4 emissions are 60% of the total CH_4 emissions [*Denman et al.*, 2007], this 15.4% decrease in total global CH_4 emissions corresponds to a 25.7% decrease in global anthropogenic CH_4 emissions. We then use the EDGAR 3.2 FT2000 anthropogenic CH_4 emission inventory [*Olivier et al.*, 2005] to estimate that NA, EU, SA, and EA each contribute 16.6%, 16.0%, 17.3%, and 19.0%, respectively, to total global anthropogenic emissions (298 Tg CH_4 a^{-1} in 2000); together the anthropogenic CH_4 emissions from these four regions contribute 68.9% to the global total anthropogenic emissions.

The fraction of the total O_3 response diagnosed from SR2-SR1 that would be produced by 20% decreases in regional anthropogenic CH_4 emissions can then be estimated (*i.e.*, for NA: (0.2*16.6% of global anthropogenic emissions)/(25.7% decrease in global anthropogenic emissions as implied by the concentration change in SR2), assuming that the O_3 response scales linearly with changes in the CH_4 burden (which is in turn proportional to changes in emissions over the range of present-day anthropogenic CH_4 emissions [*Fiore et al.*, 2008]) and that neither the magnitude of the response nor its spatial pattern depends strongly on the location of the CH_4 emission reductions, as was shown to be the case in *Fiore et al.*, [2008]. In this manner, we obtain values of 12.9%, 12.5%, 13.4%, and 14.8% of the O_3 decrease in the SR2 simulation for NA, EU, SA, and EA, respectively. We scale the ensemble mean surface O_3 response to CH_4 over the receptor regions (SR2-SR1 in Table 2) by these values to estimate an annual mean surface O_3 decrease for each SR pair (Table A6) that ranges from 0.13 ppb (EU on EA) to 0.20 ppb (EA on SA).

The results are shown in Figure 3 for comparison with the O_3 decreases achieved with reductions in the regional emissions of the traditional O_3 precursors (NO_x, NMVOC, and CO). While the combined domestic emission reductions of the traditional O_3 precursors ("ALL" in Figure 3) are most effective at reducing surface O_3 over all regions, the additional inclusion of domestic CH_4 emission reductions would yield another 14-20% decrease in annual mean surface O_3. Comparison of the "3 foreign" bars (black) in "ALL" versus "CH_4" in Figure 3 implies that the inclusion of anthropogenic CH_4 emissions in a multi-species control strategy to reduce background surface O_3 in the Northern Hemisphere would nearly double the surface O_3 decrease attained by controlling the traditional O_3 precursors alone. The larger O_3 response over foreign regions to anthropogenic CH_4 versus "ALL" O_3 precursor emissions from SA reflects the comparable amounts of anthropogenic CH_4 emissions from the four regions, whereas SA emits only half as much NO_x as the other regions. For 6 SR pairs, regional anthropogenic CH_4 emission reductions are estimated to yield equivalent (within ±25%) responses in surface O_3 over foreign continents as the coincident reductions in NO_x, NMVOC and CO (ALL). For NA on EU and EU on EA, the influence from regional CH_4 emission reductions is roughly half that of the traditional O_3 precursors, and for NA on EA and EU on SA, the CH_4 response is ~35% less than that to "ALL". The additional hemispheric-wide O_3 decrease from reductions in anthropogenic CH_4 emissions occurs on the time scale of the CH_4 perturbation time, approximately a decade, whereas the response to the traditional O_3 precursors occurs in weeks to months.

6. Response of Air Quality as Measured by Threshold Statistics

In many nations, compliance with air quality standards is assessed with respect to a threshold concentration. *Ellingsen et al.* [2008] have shown that threshold statistics based on 35, 60, and 80 ppb O_3, simulated by global CTMs, responded similarly to changes in precursor emissions across 14 world regions ($r^2 > 0.55$). Here we focus on incidences of daily maximum 8-hour average O_3 concentrations above 60 ppb (DAYS>60), a statistic used in Europe to protect human health, with a target value of 25 days or fewer per year [*e.g.*, as discussed further by *Ellingsen et al.*, 2008]. We previously showed that the model ensemble mean closely matches the monthly average O_3 observations over EU (Figure 2), and so we focus on the EMEP sites (Figure 1) to compare observed and simulated DAYS>60; results are shown in Figure 12. Over the Mediterranean and low-altitude (below 1 km) Central European regions several models (and the model ensemble mean and median) are within the observed range of DAYS>60. Consistent with the results in Figure 2, Figure 12 shows that the models tend to underestimate DAYS>60 at high-altitude central Europe with only two models simulating values within the observed range. We recommend further work to determine why some models capture this statistic better than others, including the potential role of differences in mixed layer depths and deposition.

We next explore the relevance of the monthly mean results in Figure 6 for threshold metrics. Figure 13 shows the model ensemble domain average monthly DAYS>60 in the base simulation (right axis) for each region, and the decrease in these values when all O_3 precursors are reduced by 20% in the four source regions (left axis). In the base simulation, DAYS>60 peaks in summer over NA and EU, in spring over EA, and in winter to early spring over SA (Figure 13). In all months, DAYS>60 responds most strongly to the domestic emissions reductions, with ~20% decreases in DAYS>60 during the month when the total DAYS>60 peaks (August for NA, July for EU, May for EA, and March for SA). The response of DAYS>60 to the foreign emission reductions is strongest in spring (decreases of 5-10% of the base case for some SR pairs as compared to ~15-35% decreases from domestic emission reductions during the same season). The low incidence of DAYS>60 in late fall prevents the secondary maximum shown in Figure 6 from emerging. The rankings of the O_3 responses to foreign emission decreases in spring are consistent with those in Figure 6, suggesting that the mean response qualitatively describes the response of the threshold statistics relevant for gauging attainment of air quality standards. We emphasize that the values in Figure 13 are averaged over large spatial areas and mask a large variability within the regions; for example, the model ensemble mean DAYS>60 over Europe decrease by 2-4 days over much of Southern Europe and Northern Africa, and by more than 5 days over the Middle East when ALL emissions are decreased by 20% in NA (not shown). A forthcoming manuscript [*Reidmiller et al.*, in preparation] will expand this analysis to examine variability within the United States.

The annual (spatial average) decrease in DAYS>60 attained with emission reductions in a foreign region is always <10-20% of the decrease from equivalent percentage reductions applied domestically, in contrast to the mean O_3 changes (Figure 3), in which some foreign SR pairs approach 50% of the response to domestic emissions. This result implies that DAYS>60 (and thus higher O_3 values) are more sensitive to domestic emissions, with the highest O_3 levels occurring during meteorological conditions favoring regional production from domestic emissions.

7. Evaluating the Role of Asian Emission Trends on Northern Mid-latitude Surface O_3

Observational evidence indicates that background surface O_3 at northern mid-latitudes has been increasing by 0.1-0.5 ppb yr^{-1} in recent decades [*e.g. Vingarzan*, 2004; *Carslaw*, 2005; *Jonson et al*., 2005; *Derwent et al.*, 2007; *Jaffe and Ray* 2007] although estimated trends vary and may even be leveling off [*Oltmans et al*., 2006; *Derwent et al*., 2007]. The model ensemble mean O_3 SR relationships diagnosed here can be combined with reported anthropogenic emission trends to evaluate the role of regional emission changes on Northern Hemispheric background surface O_3. While wintertime O_3 increases over Europe have been mainly attributed to decreases in EU NO_x emissions [*Jonson et al*., 2005; *Ordóñez et al*., 2005], we focus on the increase observed throughout the year, and examine whether the multi-model ensemble mean SR relationships support the hypothesis that a 0.1-0.5 ppb yr^{-1} increase in Northern Hemispheric background O_3 may be driven by precursor emissions associated with rapid industrialization in Asia [*e.g. Jaffe et al*. 2003c; *Parrish et al*., 2004]. Recent satellite retrievals of NO_2 columns suggest that NO_x emissions from China have increased by ~40%, with the growth rate accelerating from 4 to 12% per year, from 1996 to 2002 [*Richter et al*., 2005]. During this same period, little change is found over the United States, while the satellite NO_2 columns suggest a decrease of 30% over Western Europe [*Richter et al*., 2005].

The annual mean surface O_3 response to a 20% decrease in EA anthropogenic NO_x emissions from Table A4 (~0.1 ppb over the foreign regions) implies that a +10% yr^{-1} increase in EA NO_x emissions would increase O_3 by ~0.05 ppb yr^{-1}, below the observed range. If we instead assume that all Asian (*i.e*., EA+SA) emissions are increasing together with NO_x, the 20% emission reductions in Asia produce a ~0.2 (over EU) to 0.3 ppb (over NA) O_3 decrease (ALL in Table A4). In this case, the 10% yr^{-1} increase in Asian O_3 precursor emissions scales to an O_3 response that falls within the lower end of the surface O_3 increase derived from observations: an increase of 0.1 and 0.15 ppb O_3 yr^{-1}, averaged over the EU and NA receptor regions, respectively. Considering the decreases in European NO_x emissions (~5% yr^{-1}), we estimate a 0.02 and 0.03 ppb yr^{-1} annual mean decrease in surface O_3 over NA and EA, respectively, or 0.04 and 0.05 ppb yr^{-1} if EU CO and NMVOC emissions follow the EU NO_x trend. We conclude that the Asian NO_x emission changes estimated by *Richter et al.* [2005], if accompanied by increases in the other O_3 precursors over Asia, are consistent with annual mean O_3 trends of ~0.1 ppb yr^{-1}, but are insufficient to produce a 0.5 ppb yr^{-1} trend. In a similar manner, we estimate that the 60% increase in South Asian NO_x emissions projected by the Current Legislation (CLE) emission scenario between 2005 and 2030 [*Dentener et al*., 2005; *Cofala et al*., 2005] to result from growth in the power and transportation sectors would increase surface O_3 over NA, EU, and EA by less than 0.3 ppb.

Trends derived from measurements at remote sites situated on the western coasts of North America and Europe, or on mountain summits where they sample free tropospheric air, are probably not representative of the spatial average over the large continental regions considered here. The intercontinental signal at such sites may be

larger than in surface air over regions where O_3 is subjected to higher depositional and chemical loss rates. In addition to rising anthropogenic emissions, regional changes in climate, biogenic emissions and wildfires may contribute to the observed O_3 trends [*e.g.*, *Jaffe and Ray*, 2007*; Jaffe et al*., 2008]. Future studies should incorporate variability in both meteorology and emissions (including anthropogenic, biogenic, and wildfire) to explore whether models can attribute fully the observed increases in northern mid-latitude surface O_3 over the past decades, particularly given the growing demand for future projections of climate- and emission-driven changes in surface O_3.

8. Conclusions

Under the umbrella of the Task Force on Hemispheric Transport of Air Pollution (TF HTAP; www.htap.org), we have used an ensemble modeling approach to estimate the impact of precursor emissions from four continental-scale northern mid-latitude source regions on surface O_3 levels in the same four receptor regions (Figure 1). Specifically, 21 global and hemispheric chemical transport models used meteorology for 2001 to simulate the impact of 20% decreases in "conventional" O_3 precursor emissions (NO_x, NMVOC, and CO individually and combined) from East Asia (EA), Europe (EU), North America (NA) and South Asia (SA) on surface O_3 in the same four regions. Our results are intended to provide a first comprehensive assessment of annual and seasonal mean O_3 responses to changes in emissions from other continents, to gauge uncertainty in these estimates, and to serve as a benchmark for future work. The consistent approach applied in our study narrows the wide range of O_3 responses to changes in emissions on other continents reported in the literature (Figure 11). We identified a systematic model overestimate of surface O_3 concentrations compared to observations over the eastern United States and Japan (Figure 2), and show that the bias within individual models does not correlate with the strength of the O_3 response to reductions in foreign emissions. We find a strong sensitivity to uncertainties in anthropogenic NMVOC emissions, particularly over EU (Figure 10). The magnitude of simulated O_3 responses both to foreign and domestic emissions typically varies by at least a factor of two across the models (Figures 3 and 11). Reducing this uncertainty requires additional work to identify observational constraints that would distinguish which models best represent the key processes for hemispheric transport of O_3.

In addition to the precursors that are traditionally regulated to abate O_3 pollution (*i.e.*, NO_x, NMVOC, and CO), we examined the contribution of CH_4 to hemispheric-wide surface O_3 levels, both directly by changing global CH_4 abundances, and indirectly through the influence that the traditional O_3 precursors have on OH concentrations, and thereby the CH_4 abundance [*e.g. Prather*, 1996]. Due to competing effects of CO and NMVOC versus NO_x on OH, neglecting the long-term feedback when equivalent percentages of CO, NMVOC and NO_x are reduced together introduces errors of at most a few percent. Given the different anthropogenic sources of NO_x, CO, and NMVOC, application of equivalent percentage reductions to all three precursors may not be pragmatic, in which case the long-term effect may not be trivial. We further show that the responses to single-component versus multi-component emission reductions are approximately equivalent for the O_3 responses to changes in domestic and foreign

emissions (Figure 8), although the multi-component response is less-than-linear in coupled aerosol simulations in which aerosols and their precursors were also decreased. We focus the remainder of our conclusions on the simulations with the combined reductions of NO_x, CO, and NMVOC.

We define a continental-scale "import sensitivity" as the ratio of the sum of the change in surface O_3 resulting from perturbations to precursor emissions in the three foreign source regions to the surface O_3 change resulting from the same perturbations to domestic emissions. Regional O_3 production reaches a maximum in summer over EA, EU, and NA (Figure 5; ensemble regional mean O_3 decreases of 1.3-1.8 ppb), with import sensitivities for July of 0.2 (NA and EA) to 0.3 (EU) (Figure 7). We assign a high degree of uncertainty, however, to the NA and EA results given the model bias compared to surface observations during the summer and early fall (Figure 2). The model ensemble mean import sensitivity ranges from 0.5 (SA in November) to 1.1(EA in March) during the month with the largest surface O_3 response to the combined foreign emission reductions (ensemble spatial mean decrease of 0.7-0.9 ppb versus 0.8-1.6 ppb O_3 decrease from the 20% reductions in domestic anthropogenic emissions during the same month).

For all source regions, the model ensemble mean intercontinental influence is largest during spring and in late fall (Figure 6), consistent with prior studies (Figure 11 and Section 1). The most robust rankings of intercontinental influence across the models are that surface O_3 levels over EU are influenced most strongly by emission reductions in NA, followed by EA, and that SA contributes least to the three foreign regions. We find more uncertainty in the relative importance of EA versus EU on NA, and of the three source regions over both Asian regions. Our analysis of the impact of decreases in anthropogenic emissions on the incidence of daily maximum 8-hour average O_3 concentrations above 60 ppb (DAYS>60) suggests that the annual and seasonal mean responses are qualitatively relevant for assessing air quality changes as measured by a threshold statistic used to gauge compliance with air quality standards. These high O_3 values, however, are much more sensitive to domestic emissions, even in spring (domestic emission reductions yield ~15-35% decreases from the base case whereas emission reductions in individual foreign source regions yield decreases of at most 5-10%).

The annual mean responses to emission reductions of the traditional O_3 precursors from a single foreign source region are often 10% (maximum of ~50%) of the responses to domestic emission reductions (Figure 3). From the model ensemble annual mean response to a 20% decrease in global CH_4 abundances, we infer that the O_3 decrease over foreign regions produced by regional reductions in anthropogenic CH_4 emissions is roughly equivalent to the O_3 decrease from the same percentage reduction of NO_x, NMVOC, and CO together. We emphasize that these results are large spatial averages that may not convey the larger foreign influence occurring in some sub-continental regions (*e.g.* the west coasts of NA and EU). Our results provide a baseline for future assessments of the surface O_3 response to emission changes on foreign continents, a key step towards determining the interaction of domestic efforts to improve air quality with emission changes occurring elsewhere in the globe.

Acknowledgments

We are grateful to D. Jaffe and D. Reidmiller (University of Washington), and to A. Gnanadesikan and R. Stouffer (GFDL) and 3 anonymous reviewers for insightful comments on previous versions of the manuscript. CA and DB were supported primarily by the U.S. DOE Atmospheric Science Program (Office of Science, BER) at LLNL under Contract DE-AC52-07NA27344. RMD, IAM and DSS acknowledge funding from NERC (NE/D012538/1); BND from NASA MAP; MGS, KJP and WJC from the UK Defra under contract AQ902 and the Joint DECC and MoD Programme, (DECC) GA01101 (MoD) CBC/2B/0417_Annex C5; AL and JWK from the Canadian Foundation for Climate and Atmospheric Sciences, the Ontario Ministry of the Environment, the Canadian Foundation for Innovation and the Ontario Innovation Trust; and MGV from the Spanish Ministry of the Environment. RJP was partly supported by the Korea Meteorological Administration Research and Development Program under Grant CATER 2007-3205.

References

Akimoto, H. (2003), Global Air Quality and Pollution, *Science, 302*, 5651,1716-1719.

Auvray, M. and I. Bey, (2005), Long-range transport to Europe: Seasonal variations and implications for the European ozone budget, *Journal of Geophysical Research 110(D11303)*.

Bergin, M.S., J.J. West, T.J. Keating, A.G. Russell (2005), Regional Atmospheric Pollution and Transboundary Air Quality Management, *Annu. Rev. Environ. Resour.* 30:1-37,doi: 10.1146/annurev.energy.30.050504.144138

Berntsen, T.K., S. Karlsdottir, and D.A. Jaffe (1999), Influence of Asian emissions on the composition of air reaching the North Western United States, *Geophys. Res. Lett. 26*, 2172-2174.

Bey, I., D.J. Jacob, J.A. Logan, and R.M. Yantosca (2001), Asian chemical outflow to the Pacific in spring: Origins, pathways, and budgets, J. Geophys. Res., 106 (D19), 23,097-23,113.

Bowman, K.P., and G.D. Carrie (2005), The Mean-Meridional Transport Circulation of the Troposphere in an Idealized GCM, *J. Atmos. Sci., 59*, 1502-1514.

Carslaw, D.C. (2005), On the changing seasonal cycles and trends of ozone at Mace Head Ireland, Atmos. Chem. Phys., 5, 3441-3450.

Cofala, J., M. Amann, Z. Klimont, and W. Sch¨opp (2005) Scenarios of World Anthropogenic Emissions of SO2, NOx, and CO up to 2030, in Internal report of the Transboundary Air Pollution Programme, pp. 17, http://www.iiasa.ac.at/rains/global_emiss/global_emiss.html, International Institute for Applied Systems Analysis, Laxenburg, Austria.

965 Collins, W.J., D. S. Stevenson, C. E. Johnson and R. G. Derwent (2000), The European
966 regional ozone distribution and its links with the global scale for the years 1992 and 2015
967 *Atmos. Environ*., 34, 255-267.
968
969 Collins, W.J., R.G. Derwent, C.E. Johnson, and D.S. Stevenson (2002), The oxidation of
970 organic compounds in the troposphere and their global warming potentials, *Climatic*
971 *Change*, *52*, 453-479.
972
973 Cooper, O. R., and J. L. Moody, Meteorological controls on ozone at an elevated eastern
974 United States regional background monitoring site, J. Geophys. Res., 105, 6855– 6869,
975 2000.
976
977 Crutzen, P. (1973), A discussion of the chemistry of some minor constituents in the
978 stratosphere and troposphere, *Pure Appl. Geophys., 106-108*, 1385-1399.
979
980 Daniel, J.S., and S. Solomon (1998) On the climate forcing of carbon monoxide, *J.*
981 *Geophys. Res., 103*, 13,249-13,260.
982
983 Denman, K.L., et al. (2007), Couplings Between Changes in the Climate System and
984 Biogeochemistry. In: *Climate Change 2007: The Physical Science Basis, Contribution of*
985 *Working Group I to the Fourth Assessment Report of the Intergovernmental Panel on*
986 *Climate Change* [Solomon, S. and 7 others (eds.)]. Cambridge University Press,
987 Cambridge, United Kingdom and new York, NY, USA.
988
989 Dentener, F., D. Stevenson, J. Cofala, R. Mechler, M. Amann, P. Bergamaschi, F. Raes,
990 and R. Derwent (2005), The impact of air pollutant and methane emission controls on
991 tropospheric ozone and radiative forcing: CTM calculations for the period 1990-2030,
992 *Atmos. Chem. Phys.* **5,** 1731-1755.
993
994 Dentener, F., *et al*. (2006), The global atmospheric environment for the next generation,
995 *Environ. Sci. Technol., 40*, 3586-3594.
996
997 Derwent, R.G., P.G. Simmonds, S. Seuring, C. Dimmer (1998), Observation and
998 interpretation of the seasonal cycles in the surface concentrations of ozone and carbon
999 monoxide at Mace Head, Ireland from 1990 to 1994, *Atmos. Environ., 32 (2),* 145-157.
1000
1001 Derwent, R.G., W.J. Collins, C.E. Johnson, and D.S. Stevenson (2001), Transient
1002 behaviour of tropospheric ozone precursors in a global 3-D CTM and their indirect
1003 greenhouse effects, *Climatic Change*, *39*, 463-487.
1004
1005 Derwent, R. G., et al. (2002), Coupling between the global and regional scale ozone
1006 distributions over Europe and the role of intercontinental transport, presented at the
1007 USEPA/EMP workshop on hemispheric pollution.
1008

1009 Derwent, R.G., M.E. Jenkin, S.M. Saunders, M. J. Pilling, P.G. Simmonds, N.R. Passant,
1010 G.J. Dollard, P. Dumitrean, A. Kent (2003), Photochemical ozone formation in north
1011 west Europe and its control, *Atmos. Environ. 37,* 1983-1991.
1012
1013 Derwent, R. G., D. S. Stevenson, et al., (2004), Intercontinental transport and the origins
1014 of the ozone observed at surface sites in Europe, *Atmospheric Environment 38(13):* 1891-
1015 1901.
1016
1017 Derwent, R.G., P.G. Simmonds, S. O'Doherty, D.S. Stevenson, W.J. Collins, M.G.
1018 Sanderson, C.E. Johnson, F. Dentener, J. Cofala, R. Mechler, M. Ammann (2006),
1019 External influences on Europe's air quality: Baseline methane, carbon monoxide and
1020 ozone from 1990 to 2030 at Mace Head, Ireland, *Atmos. Environ., 40*, 844-855.
1021
1022 Derwent, R.G., P.G. Simmonds, A.J. Manning, T.G. Spain (2007) Trends over a 20-year
1023 period from 1987-2007 in surface ozone at the atmospheric research station, Mace Head,
1024 Ireland, *Atmos. Environ., 41*, 9091-9098.
1025
1026 Duncan, B.N., J.J. West, Y. Yoshida, A.M. Fiore, and J.R. Ziemke (2008), The
1027 influence of European pollution on ozone in the Near East and northern
1028 Africa, *Atmos. Chem. Phys., 8*, 2267-2283.
1029
1030 Ellingsen, K., M. Gauss, R. van Dingenen, F.J. Dentener, *et al*. (2008), Global ozone and
1031 air quality: a multi-model assessment of risks to human health and crops, *Atmos. Chem.*
1032 *Phys. Discuss., 8*, 2163–2223, www.atmos-chem-phys-discuss.net/8/2163/2008/
1033
1034 Fiore, A. M., D.J. Jacob, B.D. Field, D.G. Streets, S.D. Fernandes, and C. Jang (2002a),
1035 Linking Air Pollution and Climate Change: The Case for Controlling Methane, *Geophys.*
1036 *Res. Lett.* **29,** 1919.
1037
1038 Fiore, A.M., D.J. Jacob, I. Bey, R.M. Yantosca, B.D. Field, A.C. Fusco, and J.G.
1039 Wilkinson (2002b), Background ozone over the United States in summer: Origin,trend,
1040 and contribution to pollution episodes, *J. Geophys. Res., 107 (D15),*
1041 doi:10.1029/2001JD000982.
1042
1043 Fiore, A., D. J. Jacob, H. Liu, R. M. Yantosca, T. D. Fairlie, and Q. Li (2003), Variability
1044 in surface ozone background over the United States: Implications for air quality policy, *J.*
1045 *Geophys. Res., 108(D24)*, 4787, doi:10.1029/2003JD003855.
1046
1047 Fiore, A. M., J. J. West, L. W. Horowitz, V. Naik, and M. D. Schwarzkopf (2008),
1048 Characterizing the tropospheric ozone response to methane emission controls and the
1049 benefits to climate and air quality, *J. Geophys. Res., 113, D08307*,
1050 doi:10.1029/2007JD009162
1051
1052 Fuglestvedt, J. S., et al. (1999), Climatic forcing of nitrogen oxides through changes in
1053 tropospheric ozone and methane: Global model studies, Atmos. Environ., 33, 961–967.
1054

Goldstein, A. H., D. B. Millet, et al., (2004), Impact of Asian emissions on observations at Trinidad Head, California, during ITCT 2k2, *Journal of Geophysical Research 109(D23S17)*.

Guerova, G., I. Bey, J.-L. Attié, R. V. Martin, J. Cui, and M. Sprenger (2006), Impact of transatlantic transport episodes on summertime ozone in Europe, 2057-2072, SRef-ID: 1680-7324/acp/2006-6-2057.

Han, Z., et al. (2008), MICS-Asia II: Model intercomparison and evaluation of ozone and relevant species, *Atmos. Environ., 42 (15)*, 3491-3509.

Hess, P. (2005), A comparison of two paradigms: The relative global roles of moist convective versus nonconvective transport, *J. Geophys. Res., 110*, D20302, doi:10.1029/2004JD005456.

Hess, P. and J.-F. Lamarque, (2007), Ozone source attribution and its modulation by the Arctic Oscillation during the spring months, *Journal of Geophysical Research*, 112, D11303, doi:10.1029/2006JD007557.

Holloway, T., A. Fiore, and M. Galanter Hastings (2003), Intercontinental Transport of Air Pollution: Will emerging science lead to a new hemispheric treaty?, *Environ. Sci. & Technol.* , 37 (20), 4535-4542.

Holloway, T., et al. (2008), MICS-Asia II: Impact of global emissions on regional air quality in Asia, *Atmos. Environ., 42 (15)*, 3543-3561.

Holzer, M., T.M. Hall, R.B. Stull (2005), Seasonality and weather-driven variability of transpacific transport, J. Geophys. Res., 110, D23103, doi:10.1029/2005JD0006261.

Huntrieser H., et al. (2005), Intercontinental air pollution transport from North America to Europe: Experimental evidence from airborne measurements and surface observations, *J. Geophys. Res., 110, D01305*, doi:10.1029/2004JD005045.

Husar, R., et al. (2001), Asian dust events of April 1998, J. Geophys. Res., 106(D16), 18317-18330.

Jacob, D.J., L.W. Horowitz, J.W. Munger, B.G. Heikes, R.R. Dickerson, R.S. Artz, and W.C. Keene (1995), Seasonal transition from NOx- to hydrocarbon-limited conditions for ozone production over the eastern United States in September, *J. Geophys. Res., 100*, 9315-9324.

Jacob, D.J., J.A. Logan, and P.P. Murti (1999), Effect of rising Asian emissions on surface ozone in the United States, *Geophys. Res. Lett., 26*, 2175-2178.

Jaeglé L., Jaffe D.A., Price H.U., Weiss-Penzias P., Palmer P.I., Evans M.J., Jacob D.J., and Bey I (2003), Sources and budgets for CO and O_3 in the Northeast Pacific during the

spring of 2001: Results from the PHOBEA-II Experiment, *J. Geophys. Res. 108 (D20)*, 8802, doi: 10.1029/2002JD003121.

Jaffe D.A., Anderson T., Covert D., Kotchenruther R., Trost B., Danielson J., Simpson W., Berntsen T., Karlsdottir S. Blake D., Harris J., Carmichael G. and Uno I. (1999) Transport of Asian Air Pollution to North America. *Geophys. Res. Lett*. 26, 711-714.

Jaffe D., Snow J., and Cooper O. (2003a), The April 2001 Asian dust events: Transport and substantial impact on surface particulate matter concentrations across the United States. EOS transactions. Nov. 18th.

Jaffe, D.; McKendry, I.; Anderson, T.; Price H. (2003b), Six 'New' Episodes of Trans-Pacific Transport of Air Pollutants; *Atmos. Environ. 37*, 391-404.

Jaffe, D. A., D. Parrish, et al., (2003c), Increasing background ozone during spring on the west coast of North America, *Geophys. Res. Lett. 30(12):* 1613.

Jaffe, D., I. Bertschi, L. Jaeglé, P. Novelli, J. S. Reid, H. Tanimoto, R. Vingarzan, and D.L. Westphal (2004), Long-range transport of Siberian biomass burning emissions and impact on surface ozone in western North America, Geophys. Res. Lett., 31, L16106, doi:10.1029/2004GL020093.

Jaffe, D., and J. Ray (2007), Increase in surface ozone at rural sites in the western US, Atmos. Environ., 41, 5452–5463.

Jaffe D.A., Hafner W., Chand D., Westerling A., Spracklen D. (2008), Influence of Fires on O_3 Concentrations in the Western U.S. In press., Envir.Sci.Tech., April 2008.

Jonson, J. E., Simpson, D., Fagerli, H., and Solberg, S. (2005). Can we explain the trends in European ozone levels? *Atmospheric Chemistry and Physics*, *6*(1), 51-66

Keating, T. J., West, J. J. & Farrell, A. E. (2004) in Intercontinental Transport of Air Pollution, ed. Stohl, A. (Springer, Berlin), pp. 295–320.

Kunhikrishnan, T., M.G. Lawrence, R. von Kuhlmann, M.O. Wenig, A.H.Asman, A. Richter, and J.P. Burrows (2006), Regional NO_x emission strength for the Indian subcontinent and the impact of emissions from India and neighboring countries on regional O_3 chemistry, *J. Geophys. Res., 111, D15301*, doi:10.1029/2005JD006036.

Lelieveld, J. et al. (2002a), Global Air Pollution Corssroads over the Mediterranean, *Science, 298*, 794-799, doi:10.1126/science.1075457.

Lelieveld, J., W. Peters, F.J. Dentener, and M.C. Krol (2002b), Stability of tropospheric hydroxyl chemistry, J. Geophys. Res., D23, 10.1029/2002JD002272.

1146 Li, Q.B., et al. (2001), A tropospheric ozone maximum over the Middle East, Geophys.
1147 Res. Lett., 28, 3235-3238.
1148
1149 Li, Q., et al. (2002), Transatlantic transport of pollution and its effects on surface ozone
1150 in Europe and North America, *J. Geophys. Res.*, *107*, 4166, 10.1029/2001JD001422.
1151
1152 Lin, J.-T., D. J. Wuebbles, and X.-Z. Liang (2008), Effects of intercontinental transport
1153 on surface ozone over the United States: Present and future assessment with a global
1154 model, *Geophys. Res. Lett., 35, L02805*, doi:10.1029/2007GL031415.
1155
1156 Liu, H., D.J. Jacob, L.Y. Chan, S.J. Oltmans, I. Bey, R.M. Yantosca, J.M. Harris, B.N.
1157 Duncan, and R.V. Martin, Sources of tropospheric ozone along the Asian Pacific Rim:
1158 An analysis of ozonesonde observations (2002), *J. Geophys. Res., 107 (D21),*
1159 4573,10.1029/2001JD002005.
1160
1161 Liu, H.; Jacob, D.J.; Bey, I.; Yantosca, R.M.; Duncan, B.N.; Sachse G.W. Transport
1162 Pathways for Asian Pollution Outflow over the Pacific: Interannual and Seasonal
1163 Variations (2003), *J. Geophys. Res., 108*, 8786.
1164
1165 Liu, J., D. L. Mauzerall, and L. W. Horowitz (2005), Analysis of seasonal and
1166 interannual variability in transpacific transport, J. Geophys. Res., 110, D04302,
1167 doi:10.1029/2004JD005207.
1168
1169 Naik, V., D. Mauzerall, L. Horowitz, M. D. Schwarzkopf, V. Ramaswamy, and M.
1170 Oppenheimer (2005), Net radiative forcing due to changes in regional emissions of
1171 tropospheric ozone precursors, *J. Geophys. Res., 110*, D24306,
1172 doi:10.1029/2005JD005908.
1173
1174 Olivier, J. G. J., et al. (2005), Recent trends in global greenhouse gas emissions: Regional
1175 trends and spatial distribution of key sources, in Non-CO2 Greenhouse Gases (NCGG-4),
1176 edited by A. van Amstel, pp. 325– 330, Millpress, Rotterdam, Netherlands.
1177
1178 Oltmans et al. (2006), Long-term changes in tropospheric ozone, *Atmos. Environ., 40,*
1179 3156-3173.
1180
1181 Ordóñez, C., D. Brunner, J. Staehelin, P. Hadjinicolaou, J. A. Pyle, M. Jonas, H. Wernli,
1182 and A. S. H. Prévôt (2007), Strong influence of lowermost stratospheric ozone on lower
1183 tropospheric background ozone changes over Europe, Geophys. Res. Lett., 34, L07805,
1184 doi:10.1029/2006GL029113.
1185
1186 Parrish D. D., et al. (2004), Changes in the photochemical environment of the temperate
1187 North Pacific troposphere in response to increased Asian emissions, J. Geophys. Res.,
1188 109, D23S18, doi:10.1029/2004JD004978.
1189
1190 Prather, M. J. (1996), Time scales in atmospheric chemistry: Theory, GWPs for CH_4 and
1191 CO, and runaway growth, *Geophys. Res. Lett., 23*, 2597-2600.

Prather, M., et al. (2001), in *Climate Change 2001: The Scientific Basis*, eds. Houghton, J. T., Ding, Y., Griggs, D. J., Noguer, M., van der Linden, P. J., Dai, X., Maskell, K. & Johnson, C. A. (Cambridge University Press, Cambridge), pp. 239-287.

Prinn, R.G. et al. (2005), Evidence for variability of atmospheric hydroxyl radicals over the past quarter century, Geophys. Res. Lett., 32, L07809, doi:10.1029/2004GL022228.

Prospero, J. M. (1999), Long-term measurements of the transport of African mineral dust to the southeastern United States: Implications for regional air quality, *Journal of Geophysical Research-Atmospheres 104(D13):* 15917-15927.

Pochanart P., H. Akimoto, Y. Kajii, V. M. Potemkin, and T. V. Khodzher (2003), Regional background ozone and carbon monoxide variations in remote Siberia/East Asia, J. Geophys. Res., 108 (D1), 4028, doi:10.1029/2001JD001412.

Reichler, T., and J. Kim (2008), How Well do Coupled Models Simulate Today's Climate?, *Bull. Amer. Meteor. Soc., 89*, 303-311.

Richter, A., J. P. Burrows, et al., (2005), Increase in tropospheric nitrogen dioxide over China observed from space, *Nature 437(7055):* 129-132.

Sanderson, M., et al (2008), A multi-model study of the hemispheric transport and deposition of oxidised nitrogen, *Geophys. Res. Lett., 35*, L17815, doi:10.1029/2008GL035389.

Schultz, M.G., et al. (2007), REanalysis of the TROpospheric (RETRO) chemical composition over the past 40 years, Report no. 48/2007 in the series "Reports on Earth System Science" of the Max Planck Institute for Meteorology, Hamburg, ISSN 1614-1199.

Schulz, M., et al. (2006), Radiative forcing by aerosols as derived from the AeroCom present-day and pre-industrial simulations, Atmos. Chem. Phys., 6, 5225-5246.

Shindell, D. et al. (2008), A multi-model assessment of pollution transport to the Arctic, *Atmos. Chem. Phys., 8*, 5353-5372.

Sillman, S. (1999), The relation between ozone, NO_x and hydrocarbons in urban and polluted rural environments. Millenial Review series, *Atmos. Environ., 33*, 12, 1821-1845.

Solberg, S., R.G. Derwent, O. Hov, J. Langner, and A. Lindskog (2005), European Abatement of Surface Ozone in a Global Perspective, *Ambio, 34 (1)*, pp. 47-53.

Spivakovsky, C.M., et al. (2000), Three-dimensional climatological distribution of tropopsheric OH: Update and evaluation, *J. Geophys. Res., 105 (D7)*, 8931-8980.

Stevenson, D.S., R.M. Doherty, M.G. Sanderson, W.J. Collins, C.E. Johnson, and R.G. Derwent (2004), Radiative forcing from aircraft NO_x emissions: Mechanisms and seasonal dependence, *J. Geophys. Res., 109, D17307*, doi:10.1029/2004JD004759.

Stevenson, D.S., et al. (2006), Multi-model ensemble simulations of present-day and near-future tropospheric ozone, *J. Geophys. Res., 111*, D08301, doi:10.1029/2005JD006338.

Stohl A., S. Eckhardt, C. Forster, P. James, and N. Spichtinger (2002), On the pathways and timescales of intercontinental air pollution transport, *J. Geophys. Res., 107 (D23)*, 4684, doi:10.1029/2001JD001396.

Sudo K., H. Akimoto (2007), Global source attribution of tropospheric ozone: Long-range transport from various source regions, J. Geophys. Res., 112, D12302, doi:10.1029/2006JD007992.

Szopa, S., et al., (2006), Future global tropospheric ozone changes and impact on European air quality, *Geophysical Research Letters 33(L14805)*.

Task Force on Hemispheric Transport of Air Pollution (TF HTAP) (2007), Hemispheric Transport of Air Pollution 2007 Interim Report, Air Pollution Studies No. 16, T.J. Keating and A. Zuber (eds). United Nations Economic Commission for Europe, New York and Geneva, available at www.htap.org.

Trickl T., O. R. Cooper, H. Eisele, P. James, R. Mücke, A. Stohl (2003), Intercontinental transport and its influence on the ozone concentrations over central Europe: Three case studies, J. Geophys. Res., 108 (D12), 8530, doi:10.1029/2002JD002735.

Vingarzan, R. (2004), A review of surface ozone background levels and trends, *Atmos. Environ., 38* (21), p.3431-3442.

Wang, Y., D.J. Jacob, and J.A. Logan (1998), *Global simulation of tropospheric O_3-NO_x-hydrocarbon chemistry, 3. Origin of tropospheric ozone and effects of non-methane hydrocarbons*, J. Geophys. Res., 103/D9, 10,757-10,768.

Wang, Y., and D.J. Jacob (1998), Anthropogenic forcing on tropospheric ozone and OH since preindustrial times, *J. Geophys. Res., 103*, 31,123-31,135.

Weiss-Penzias P., D. A. Jaffe, L. Jaeglé, Q. Liang (2004), Influence of long-range-transported pollution on the annual and diurnal cycles of carbon monoxide and ozone at Cheeka Peak Observatory, J. Geophys. Res., 109, D23S14, doi:10.1029/2004JD004505.

Weiss-Penzias, P., D. A. Jaffe, P. Swartzendruber, J. B. Dennison, D. Chand, W. Hafner, and E. Prestbo (2006), Observations of Asian air pollution in the free troposphere at Mount Bachelor Observatory during the spring of 2004, J. Geophys. Res.,

111, D10304, doi:10.1029/2005JD006522.

West, J. J., A. M. Fiore, V. Naik, L.W. Horowitz, M.D. Schwarzkopf, D.L. Mauzerall (2007a), Ozone air quality and radiative forcing consequences of changes in ozone precursor emissions, *Geophys. Res. Lett., 34* , L06806, 10.1029/2006GL029173.

Wild, O. and M.J.Prather (2000), Excitation of the primary tropospheric chemical mode in a global three-dimensional model, *J. Geophys. Res., 105 (D20)*, 24,647-24,660.

Wild, O. and H. Akimoto, (2001), Intercontinental transport of ozone and its precursors in a three dimensional globe CTM, *J. Geophys. Res. 106(D21):* 27729-27744.

Wild, O., M. J. Prather, and H. Akimoto (2001), Indirect long-term global radiative cooling from NO_x Emissions, Geophys. Res.Lett., 28, 1719– 1722.

Wild, O., J.K. Sundet, M.J. Prather, I.S.A. Isaksen, H. Akimoto, E.V. Browell, and S.J. Oltmans (2003), CTM Ozone Simulations for Spring 2001 over the Western Pacific: Comparisons with TRACE-P lidar, ozonesondes and TOMS columns, J. Geophys. Res., 108, 8826, doi:10.1029/2002JD003283.

Wild, O., *et al*., (2004), Trans-Eurasian transport of ozone and its precursors, *Journal of Geophysical Research 109(D11302)*.

Wild, O. (2007), Modelling the global tropospheric ozone budget: exploring the variability in current models, *Atmos. Chem. Phys., 7*, 2643-2660.

Wilkening, K. E., L. A. Barrie, et al., (2000), Atmospheric Science: Trans-Pacific Air Pollution, *Science 290(5489):* 65-67.

World Health Organization (WHO), (2005), WHO air quality guidelines global update, report on a working group meeting, Bonn, Germany, 18-20 October, 2005, report number E87950.

Wu, S., L.J. Mickley, D.J. Jacob, J.A. Logan, R.M. Yantosca, and D. Rind (2007), Why are there large differences between models in global budgets of tropospheric ozone?, J. Geophys. Res., 112, D05302, doi:10.1029/2006JD007801.

Yienger, J., M. Galanter, T. Holloway, M. Phadnis, S. Guttikunda, G. Carmichael, W. Moxim, and H. Levy II (2000), The episodic nature of air pollution transport from Asia to North America, J. Geophys. Res., 105(D22), 26931-26945.

FIGURE CAPTIONS

Figure 1. The HTAP source-receptor regions: NA (15-55°N; 60-125°W), EU (25-65°N; 10°W-50°E), EA (15-50°N; 95-160°E), and SA (5-35°N; 50-95°E). Sites marked with the same symbols are used to produce the sub-regional averages in Figure 2, from the European Monitoring and Evaluation Programme (EMEP) in the Mediterannean (red diamonds; Figure 2a) and Central Europe (green open triangles for sites below 1 km and blue crosses for sites > 1 km; 2b and 2c, respectively); from the U.S. Clean Air Status and Trends Network (CASTNet) in the Northeast (red circles; 2d) Southwest (green triangles; 2e), Southeast (dark blue inverted triangles; 2f), Great Lakes (pink diamonds; 2g), Mountainous West (cyan squares; 2h), and from the Acid Deposition Monitoring Network in East Asia (EANET) in Japan (red asterisks; 2i).

Figure 2. Monthly mean surface O_3 concentrations (ppb) for the year 2001. Observed values (black circles) represent the average of all sites falling within the given latitude, longitude, and altitude boundaries and denoted by the colored symbols in Figure 1; vertical black lines depict the standard deviation across the sites. Monthly mean O_3 in the surface layer of the SR1 simulations from the 21 models are first sampled at the model grid cells containing the observational sites, and then averaged within sub-regions (grey lines); these spatial averages from each model are used to determine the multi-model ensemble median (solid red line) and mean (blue dashed line). Observations are from CASTNET (http://www.epa.gov/castnet/ozone.html) in the USA, from EMEP (http://www.nilu.no/projects/ccc/emepdata.html) in Europe, and from EANET (http://www.eanet.cc/eanet.html) in Japan.

Figure 3. Model ensemble surface O_3 response (ppb), annually and spatially averaged over the receptor regions (Figure 1) to 20% reductions of anthropogenic O_3 precursor emissions individually (NO_x, NMVOC, and CO), combined (ALL), and CH_4 within the source regions (see also Table A4). Each group of bars includes results from the four regional perturbation experiments: NA (red), EU (green), EA (dark blue) and SA (cyan), as well as the sum of the impacts from the 3 foreign source regions (black bar). The responses to the global CH_4 level reduction are estimated as described in Section 5.3 using the model ensemble mean results from SR1-SR2 (Table A4). The whiskers span the full range of the individual model responses.

Figure 4. Decrease in monthly mean surface O_3 over the receptor regions (one per panel) resulting from 20% reductions in anthropogenic O_3 precursor emissions within the same region: NO_x (SR1-SR3; red), VOC (SR1-SR4; green), CO (SR1-SR5; blue) and combined (ALL; SR1-SR6; black). Model ensemble means are shown for all available model results (filled circles; see Table A4 for the number of models contributing to each simulation) and for the subset of models in Table 2 (solid lines). The dotted line shows the model ensemble mean total O_3 response for the models in Table 2 (using all available simulations although not all models conducted every simulation) after accounting for the long-term impact from changes in CH_4 (see Section 5.2 for details) and shows little change from the short-term results.

Figure 5. Same as Figure 4, but for the sum of the O_3 decreases in the 3 simulations in which anthropogenic emissions were reduced by 20% in the foreign source regions. Note that a change in scale from Figure 4 is necessary for the ordinate axis given the smaller responses to foreign emissions.

Figure 6. Combined decrease in the 15-model ensemble monthly mean surface O_3 over the receptor regions (one per panel) resulting from simultaneous 20% decreases in all anthropogenic O_3 precursor emissions in the 3 foreign source regions (SR1-SR6). The black line for "ALL" is identical to the black circles in Figure 5).

Figure 7. Monthly mean import sensitivities for each region (IS_r; where r = NA (red), EU (green), EA (blue) and SA (cyan)) for the simulations with simultaneous 20% decreases in anthropogenic NO_x, CO, and NMVOC emissions (ALL), calculated as described in Section 4.1. Not shown are the values >2 for IS_{NA} (December and January) and IS_{EU} (November and February) which result from the small wintertime domestic responses, nor the negative values for IS_{EU} (December and January) which result from O_3 titration by EU NO_x emissions (see domestic responses in Figure 4).

Figure 8. Multi-model spatial average decrease in surface O_3 over the receptor regions resulting from 20% reductions in the O_3 precursor emissions in the 3 foreign (top panel) and domestic source regions (bottom panel) for the season of peak sensitivity to those emissions (determined from Figures 5 and 4, respectively) in those models where aerosol emission reductions are not included in SR6 (FRGSC/UCI, GEMAQ-v1p0, STOC-HadAM3-v01, and UM-CAM-v01). Each color in the top panel represents a summation of the model ensemble mean surface O_3 responses to the emission perturbations in the 3 foreign source regions.

Figure 9. Change in spatial average surface O_3 over the EU (left) and NA (right) as a function of various size perturbations to EU anthropogenic NO_x emissions by season (colors), as simulated with the FRSGC/UCI model (solid lines with circles) and as estimated by scaling linearly from the response in the simulation where NO_x emissions were decreased by 20% (SR3EU; dotted lines).

Figure 10. Decrease in annual spatial mean NA surface O_3 (ppb) resulting from 20% reductions in EU anthropogenic NMVOC emissions (SR1-SR4EU) plotted against the EU anthropogenic NMVOC emissions (Tg C a^{-1}). The points represent the results from individual models. EU anthropogenic NMVOC emissions are given in Table A3 for each model. The coefficient of determination (r^2) is 0.50.

Figure 11. Annual and seasonal mean contribution to total surface O_3 from foreign source regions as estimated from the individual model results in this study (colored by source region: green for EU; blue for EA, grey for EA+EU; red for NA) and from studies in the published literature (thin vertical bars for ranges across studies and regions; squares where one value is reported; note that regional definitions, methods for source attribution, and reported metrics (e.g. 24-hour vs. afternoon vs. daytime mean) vary across studies) [*Derwent et al*., 1998; *Berntsen et al*., 1999; *Wild and Akimoto*, 2001;

Derwent et al., 2002; *Fiore et al.*, 2002b; *Jaeglé et al*., 2003; *Li et al*., 2002; *Liu et al.*, 2002; *Pochanart et al.*, 2003; *Derwent et al.*, 2004; *Wild et al*., 2004; *Auvray and Bey*, 2005; *Guerova et al.*, 2006; *Sudo and Akimoto*, 2007; *Duncan et al.*, 2008; *Holloway et al.*, 2008; *Lin et al*., 2008] All results are scaled to 100% contributions as in Table 5-2 of *TF HTAP*, 2007. The contributions from this work are estimated by linearly scaling the simulated surface O_3 response to the combined 20% decreases in anthropogenic emissions of NO_x, CO, and NMVOC in the foreign source regions to 100% decreases, *i.e.*, 5*(SR1-SR6). The white circles represent the multi-model median value.

Figure 12: Observed (black circles) and simulated (grey diamonds) annual number of days when daily maximum 8-hour average O_3 concentrations exceed 60 ppb at the EMEP stations, averaged over the regions in Figure 2: Mediterranean (Medit.), Central European sites below 1 km altitude (C EU < 1km) and above 1 km altitude (C EU > 1km). The black vertical bars depict the standard deviation of the observed values across the stations within the region. The model ensemble mean (red circles) and median (green circles) values from the 18 models that contributed hourly surface O_3 results for SR1 are also shown.

Figure 13. Decrease in the model ensemble average number of days per month when daily maximum 8-hour average O_3 concentrations exceed 60 ppb resulting from simultaneous 20% reductions in anthropogenic NO_x, CO, and NMVOC emissions within the source regions (colored lines; red = NA; green = EU; dark blue = EA; light blue = SA), spatially averaged over each receptor region (panels). Also shown are the model ensemble average DAYS>60 in the base case SR1 simulation for each region (black lines; right axes as indicated by arrows). The change is estimated by first calculating the area-weighted spatial average value for DAYS>60 in each model simulation for a given region,and then taking the multi-model average of the differences in these spatially averaged DAYS>60 values (SR1-SR6). Hourly surface O_3 values are taken from the SR6 and SR1 simulations in 13 models: CAMCHEM, ECHAM5-HAMMOZ, EMEP, FRSGC/UCI, GEMAQ-v1p0, GEOS-Chem-v07, GMI, LMDz3-INCA1, LLNL-IMPACT, MOZARTGFDL, MOZECH, TM5-JRC-cy2-ipcc, UM-CAM.

Table 1. Model ensemble annual mean (median) ± one standard deviation in total and anthropogenic emissions of NO_x (Tg N a^{-1}), NMVOC (Tg C a^{-1}), and CO (Tg a^{-1}), globally and for the regions in Figure 1. Emissions in individual models are provided in Tables A2 and A3.

Total Emis.	GLOBAL	NA	EU	EA	SA
NO_x	46.5(46.2)±5.7	8.5(8.7)±0.8	8.4(8.4)±1.1	7.1(6.9)±1.4	3.3(3.3)±0.5
NMVOC	630(623)±221	62(57)±24	37(34)±13	48(47)±14	33(34)±8.8
CO	1060(1090)±135	130(130)±20	90(81)±25	150(150) ±29	97(96)±23
Anthr. Emis.					
NO_x	32.5(29.4)±6.0	7.4(7.3)±0.4	7.3(7.5)±0.6	6.0(5.5)±1.4	2.4(2.2)±0.4
NMVOC	96.8(92.3)±41.8	16(16)±7.0	19(20)±11	16(17)±6.5	10(10)±3.9
CO	661(563)±214	101(103)±19	80(70)±23	133(123) ±35	80(79)±18

Table 2. Methane lifetime (τ) and "feedback factor" (F) in the individual models

MODEL	τ_{OH} [a]	τ_{tot} [b]	F [c]
CAMCHEM-3311m13	11.86	10.11	1.30
FRSGCUCI-v01	8.70	7.72	1.43
GISS-PUCCINI_modelE	10.88	9.39	1.36
GMI-v02f	10.38	9.02	1.31
LMDz3-INCA1	10.02	8.74	1.31
LLNL_IMPACT-T5a	6.19	5.68	1.40
MOZARTGFDL-v2	10.44	9.06	1.31
MOZECH-v16	11.20	9.63	1.29
STOC-HadAM3	9.31	8.20	1.31
STOCHEM-HadGEM	11.72	10.01	1.28
TM5-JRC-cy2-ipcc-v1	9.02	7.97	1.43
UM-CAM-v01	12.50	10.57	1.25
Model Ensemble Mean	**10.19**	**8.84**	**1.33**
Standard Deviation	**1.72**	**1.33**	**0.06**

[a] The CH_4 lifetime against loss by tropospheric OH (years), defined as the total atmospheric burden divided by the tropospheric CH_4 loss rates, with the troposphere defined using the 150 ppb O_3 chemical tropopause.

[b] The total atmospheric CH_4 lifetime (years) determined from τ_{OH} and assuming CH_4 losses to soils and the stratosphere with lifetimes of 160 and 120 years [*Prather et al.*, 2001], respectively.

[c] The feedback factor is the ratio of the atmospheric response (or perturbation) time to the global atmospheric lifetime and is given by 1/(1-s) where *s* is determined from the SR2 and SR1 simulations, and defined as $\delta \ln(\tau) / \delta \ln[CH_4]$ [*Prather et al.*, 2001], where $[CH_4]$ = 1760 ppb in SR1 and 1408 ppb in SR2.

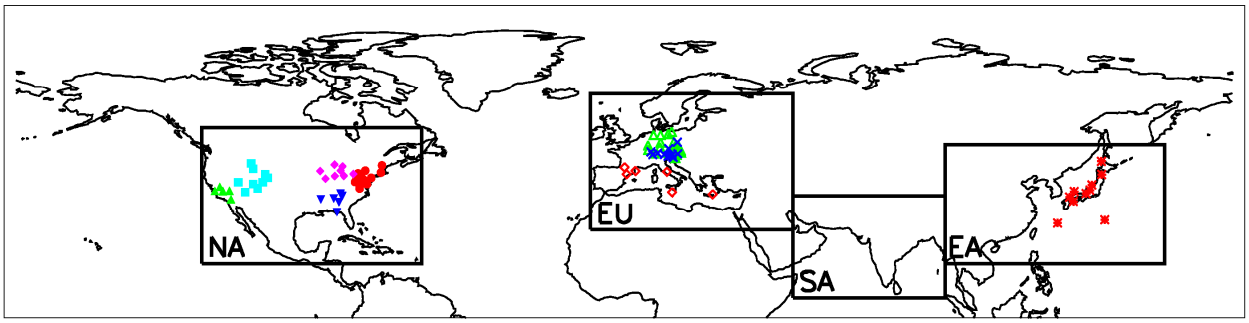

Figure 1. The HTAP source-receptor regions: NA (15-55°N; 60-125°W), EU (25-65°N; 10°W-50°E), EA (15-50°N; 95-160°E), and SA (5-35°N; 50-95°E). Sites marked with the same symbols are used to produce the sub-regional averages in Figure 2, from the European Monitoring and Evaluation Programme (EMEP) in the Mediterannean (red diamonds; Figure 2a) and Central Europe (green open triangles for sites below 1 km and blue crosses for sites > 1 km; 2b and 2c, respectively); from the U.S. Clean Air Status and Trends Network (CASTNet) in the Northeast (red circles; 2d) Southwest (green triangles; 2e), Southeast (dark blue inverted triangles; 2f), Great Lakes (pink diamonds; 2g), Mountainous West (cyan squares; 2h), and from the Acid Deposition Monitoring Network in East Asia (EANET) in Japan (red asterisks; 2i).

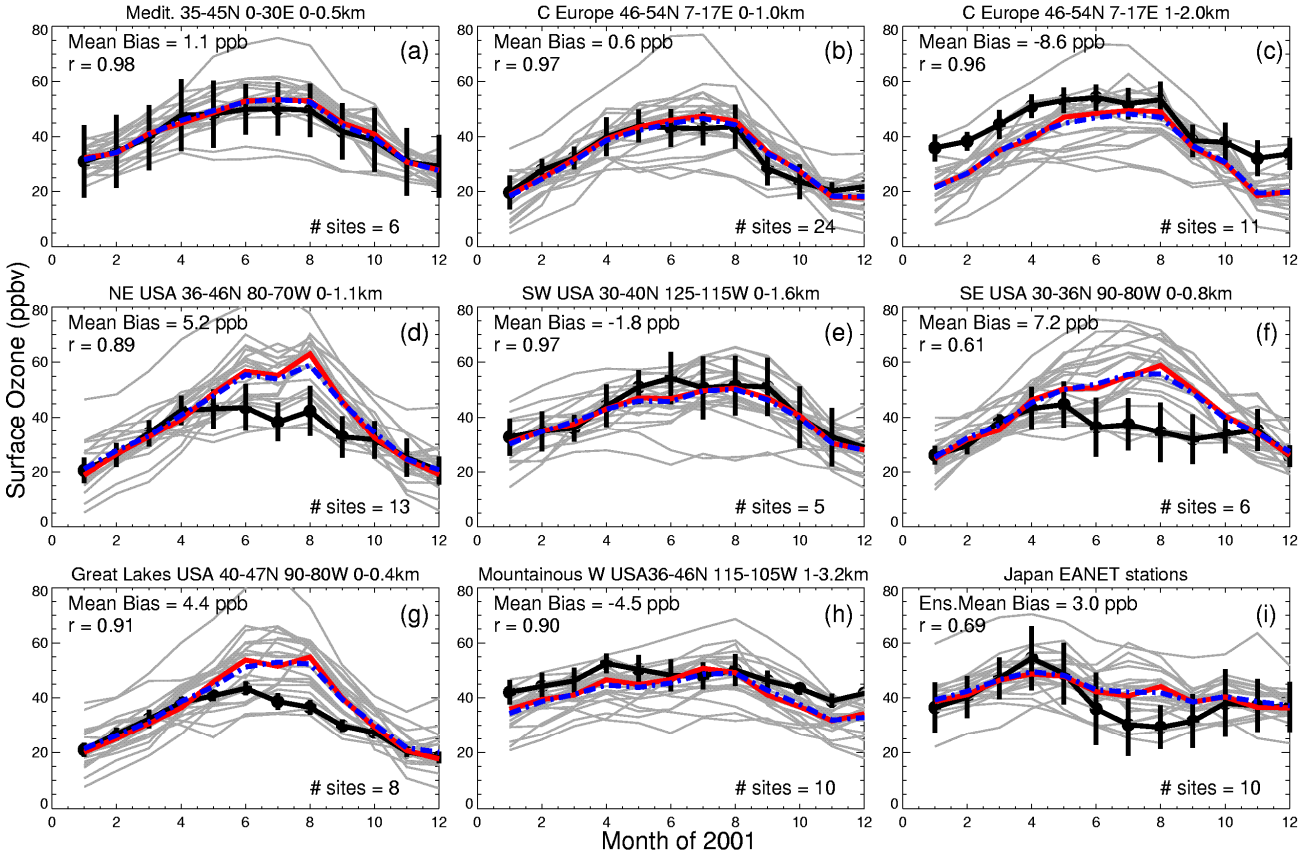

Figure 2. Monthly mean surface O_3 concentrations (ppb) for the year 2001. Observed values (black circles) represent the average of all sites falling within the given latitude, longitude, and altitude boundaries and denoted by the colored symbols in Figure 1; vertical black lines depict the standard deviation across the sites. Monthly mean O_3 in the surface layer of the SR1 simulations from the 21 models are first sampled at the model grid cells containing the observational sites, and then averaged within sub-regions (grey lines); these spatial averages from each model are used to determine the multi-model ensemble median (solid red line) and mean (blue dashed line). Observations are from CASTNET (http://www.epa.gov/castnet/ozone.html) in the USA, from EMEP (http://www.nilu.no/projects/ccc/emepdata.html) in Europe, and from EANET (http://www.eanet.cc/eanet.html) in Japan.

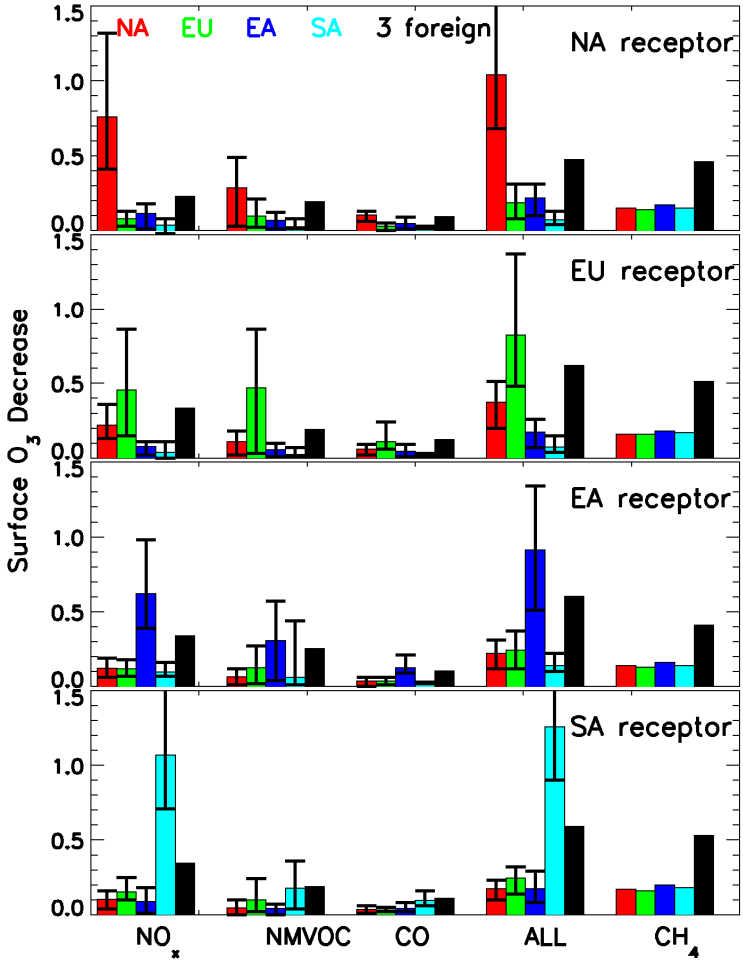

Figure 3. Model ensemble surface O_3 response (ppb), annually and spatially averaged over the receptor regions (Figure 1) to 20% reductions of anthropogenic O_3 precursor emissions individually (NO_x, NMVOC, and CO), combined (ALL), and CH_4 within the source regions (see also Table A4). Each group of bars includes results from the four regional perturbation experiments: NA (red), EU (green), EA (dark blue) and SA (cyan), as well as the sum of the impacts from the 3 foreign source regions (black bar). The responses to the global CH_4 level reduction are estimated as described in Section 5.3 using the model ensemble mean results from SR1-SR2 (Table A4). The whiskers span the full range of the individual model responses.

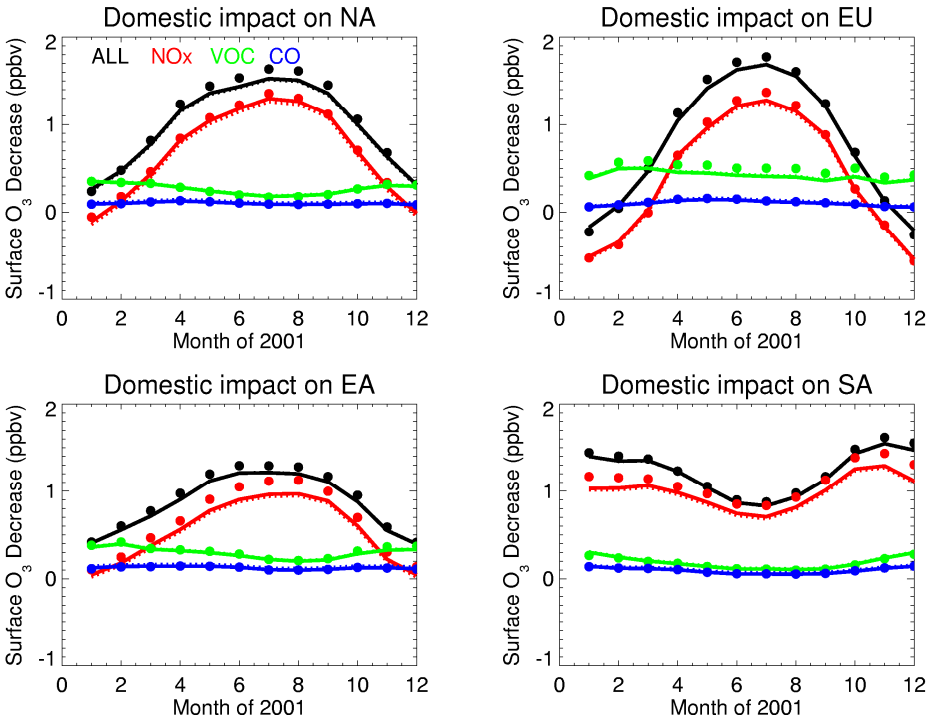

Figure 4. Decrease in monthly mean surface O_3 over the receptor regions (one per panel) resulting from 20% reductions in anthropogenic O_3 precursor emissions within the same region: NO_x (SR1-SR3; red), VOC (SR1-SR4; green), CO (SR1-SR5; blue) and combined (ALL; SR1-SR6; black). Model ensemble means are shown for all available model results (filled circles; see Table A4 for the number of models contributing to each simulation) and for the subset of models in Table 2 (solid lines). The dotted line shows the model ensemble mean total O_3 response for the models in Table 2 (using all available simulations although not all models conducted every simulation) after accounting for the long-term impact from changes in CH_4 (see Section 5.2 for details) and shows little change from the short-term results.

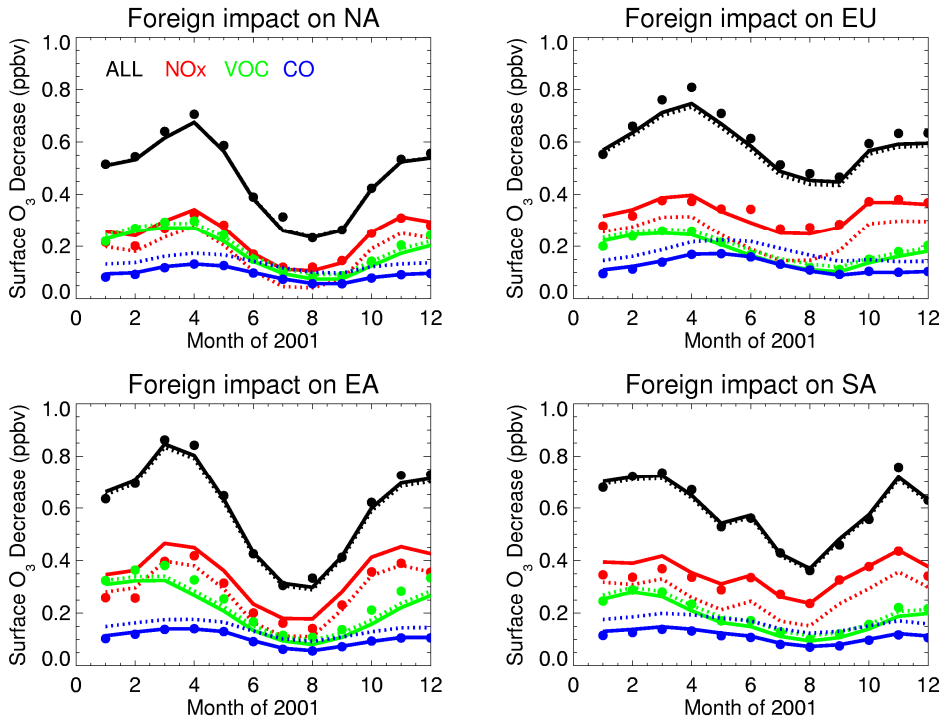

Figure 5. Same as Figure 4, but for the sum of the O_3 decreases in the 3 simulations in which anthropogenic emissions were reduced by 20% in the foreign source regions. Note that a change in scale from Figure 4 is necessary for the ordinate axis given the smaller responses to foreign emissions.

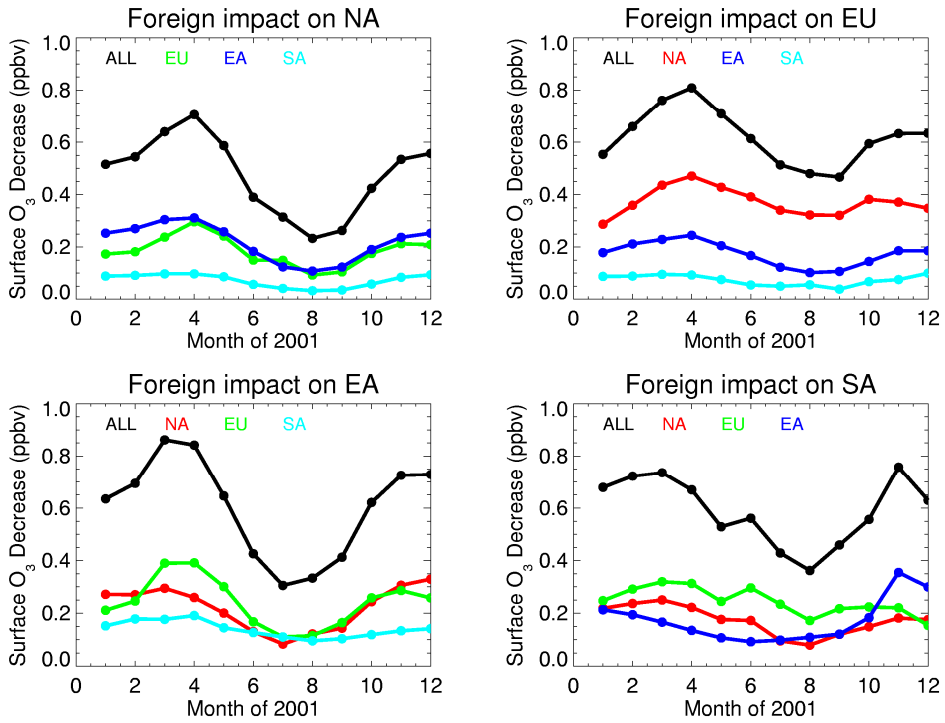

Figure 6. Combined decrease in the 15-model ensemble monthly mean surface O_3 over the receptor regions (one per panel) resulting from simultaneous 20% decreases in all anthropogenic O_3 precursor emissions in the 3 foreign source regions (SR1-SR6). The black line for "ALL" is identical to the black circles in Figure 5).

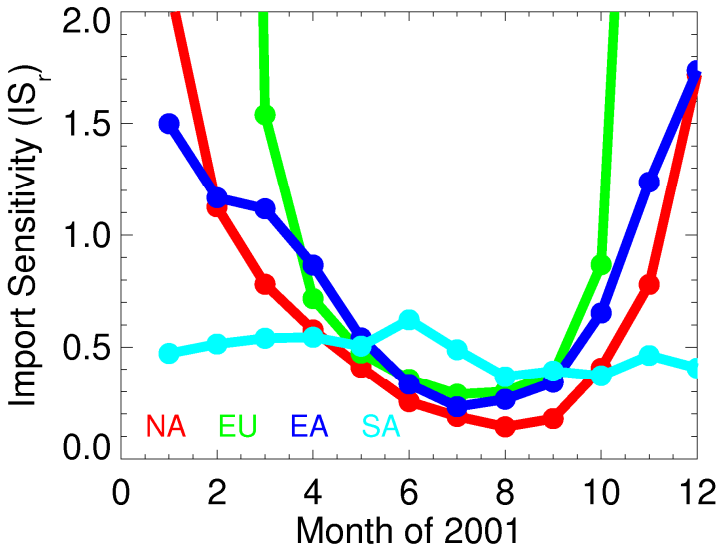

Figure 7. Monthly mean import sensitivities for each region (IS_r; where r = NA (red), EU (green), EA (blue) and SA (cyan)) for the simulations with simultaneous 20% decreases in anthropogenic NO_x, CO, and NMVOC emissions (ALL), calculated as described in Section 4.1. Not shown are the values >2 for IS_{NA} (December and January) and IS_{EU} (November and February) which result from the small wintertime domestic responses, nor the negative values for IS_{EU} (December and January) which result from O_3 titration by EU NO_x emissions (see domestic responses in Figure 4).

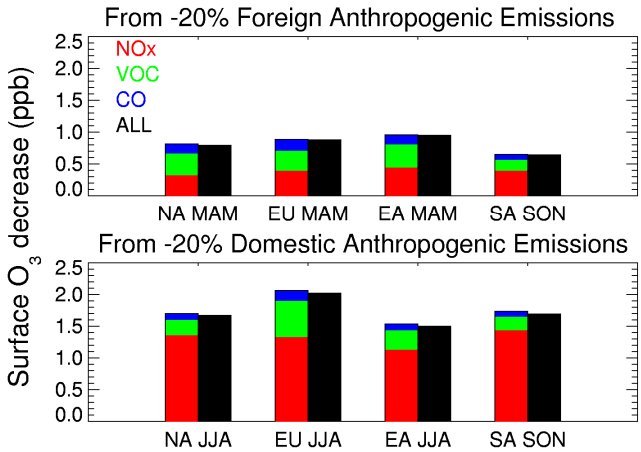

Figure 8. Multi-model spatial average decrease in surface O_3 over the receptor regions resulting from 20% reductions in the O_3 precursor emissions in the 3 foreign (top panel) and domestic source regions (bottom panel) for the season of peak sensitivity to those emissions (determined from Figures 5 and 4, respectively) in those models where aerosol emission reductions are not included in SR6 (FRGSC/UCI, GEMAQ-v1p0, STOC-

HadAM3-v01, and UM-CAM-v01). Each color in the top panel represents a summation of the model ensemble mean surface O_3 responses to the emission perturbations in the 3 foreign source regions.

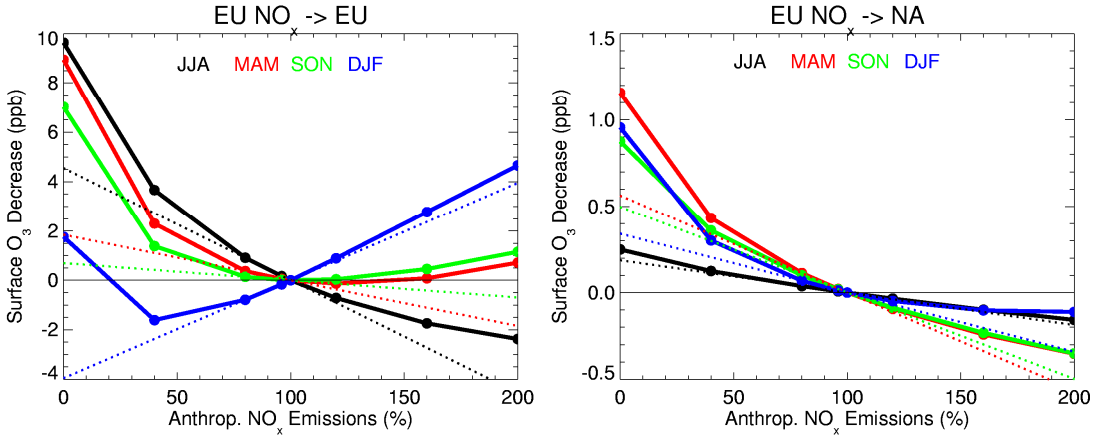

Figure 9. Change in spatial average surface O_3 over the EU (left) and NA (right) as a function of various size perturbations to EU anthropogenic NO_x emissions by season (colors), as simulated with the FRSGC/UCI model (solid lines with circles) and as estimated by scaling linearly from the response in the simulation where NO_x emissions were decreased by 20% (SR3EU; dotted lines).

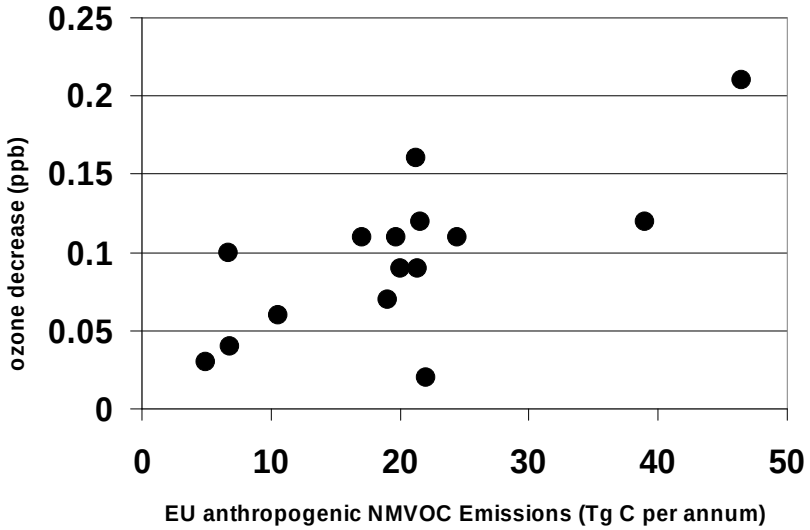

Figure 10. Decrease in annual spatial mean NA surface O_3 (ppb) resulting from 20% reductions in EU anthropogenic NMVOC emissions (SR1-SR4EU) plotted against the EU anthropogenic NMVOC emissions (Tg C a^{-1}). The points represent the results from individual models. EU anthropogenic NMVOC emissions are given in Table A3 for each model. The coefficient of determination (r^2) is 0.50.

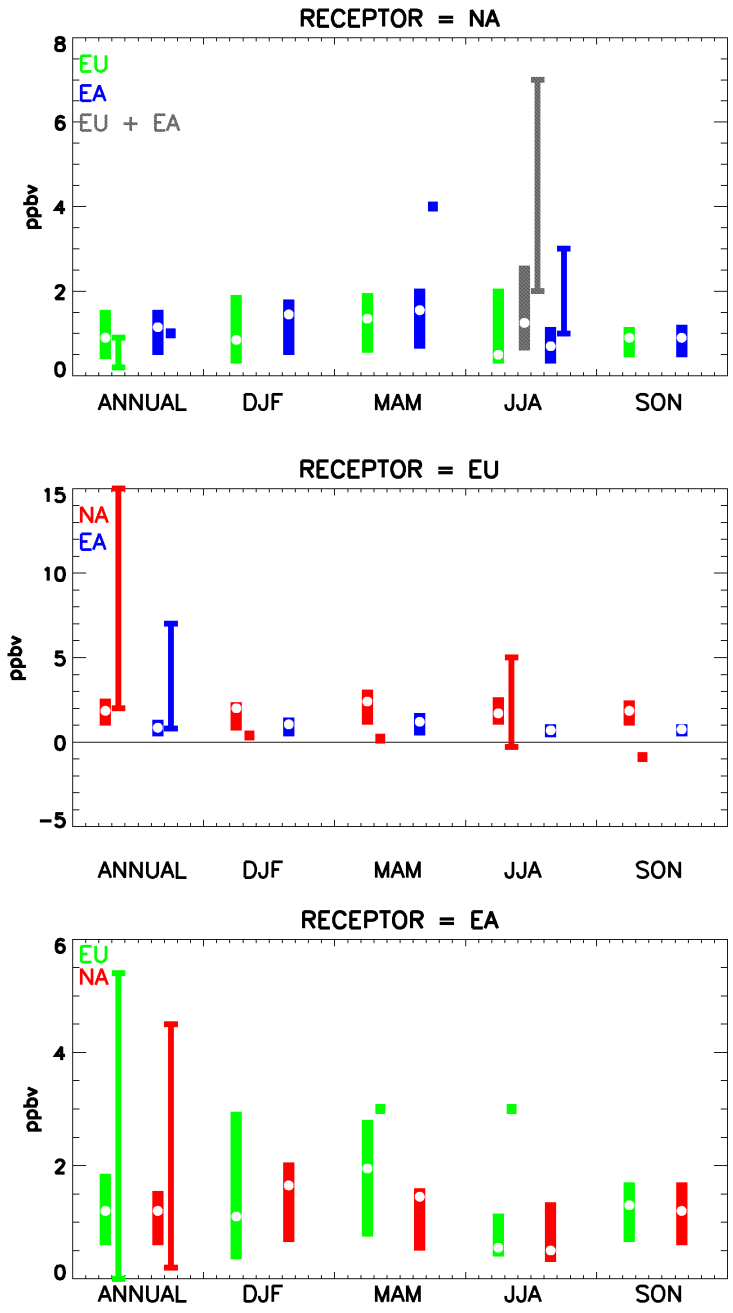

Figure 11. Annual and seasonal mean contribution to total surface O_3 from foreign source regions as estimated from the individual model results in this study (colored by source region: green for EU; blue for EA, grey for EA+EU; red for NA) and from studies in the published literature (thin vertical bars for ranges across studies and regions; squares where one value is reported; note that regional definitions, methods for source attribution, and reported metrics (e.g. 24-hour vs. afternoon vs. daytime mean) vary across studies) [*Derwent et al.*, 1998; *Berntsen et al.*, 1999; *Wild and Akimoto*, 2001; *Derwent et al.*, 2002; *Fiore et al.*, 2002b; *Jaeglé et al.*, 2003; *Li et al.*, 2002; *Liu et al.*,

2002; *Pochanart et al.*, 2003; *Derwent et al.*, 2004; *Wild et al.*, 2004; *Auvray and Bey*, 2005; *Guerova et al.*, 2006; *Sudo and Akimoto*, 2007; *Duncan et al.*, 2008; *Holloway et al.*, 2008; *Lin et al.*, 2008] All results are scaled to 100% contributions as in Table 5-2 of *TF HTAP*, 2007. The contributions from this work are estimated by linearly scaling the simulated surface O_3 response to the combined 20% decreases in anthropogenic emissions of NO_x, CO, and NMVOC in the foreign source regions to 100% decreases, *i.e.*, 5*(SR1-SR6). The white circles represent the multi-model median value.

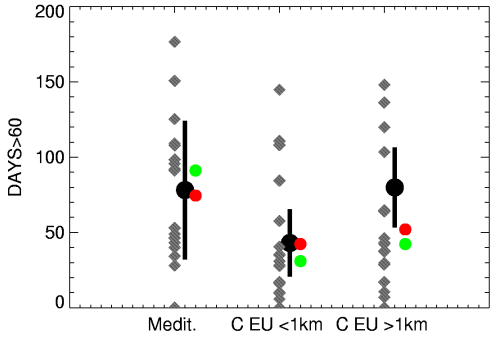

Figure 12: Observed (black circles) and simulated (grey diamonds) annual number of days when daily maximum 8-hour average O_3 concentrations exceed 60 ppb at the EMEP stations, averaged over the regions in Figure 2: Mediterranean (Medit.), Central European sites below 1 km altitude (C EU < 1km) and above 1 km altitude (C EU > 1km). The black vertical bars depict the standard deviation of the observed values across the stations within the region. The model ensemble mean (red circles) and median (green circles) values from the 18 models that contributed hourly surface O_3 results for SR1 are also shown.

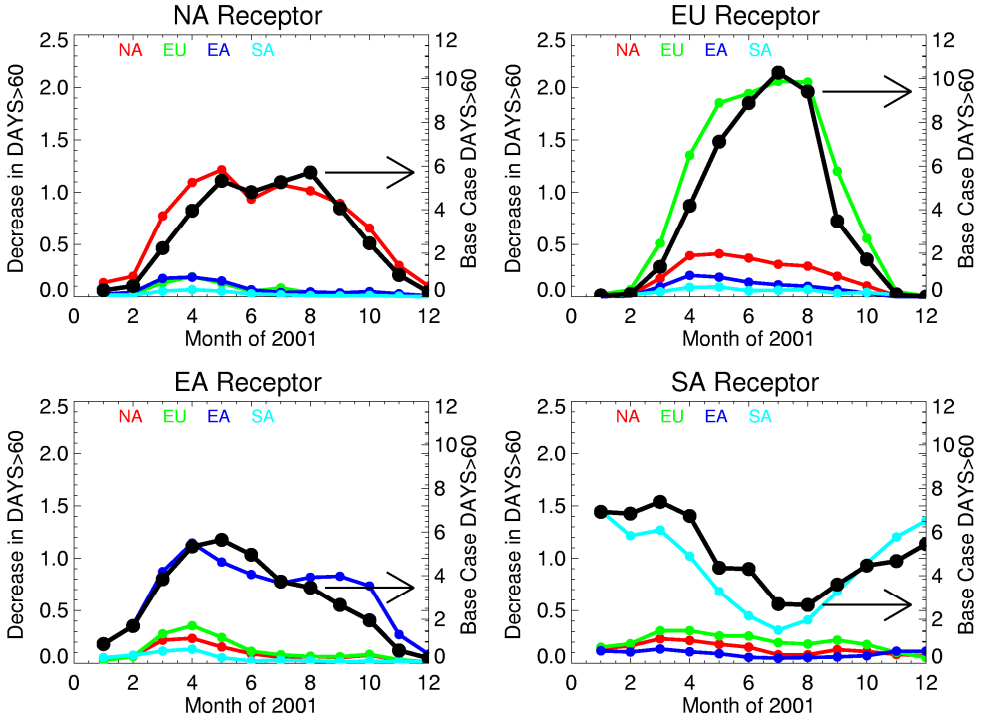

Figure 13. Decrease in the model ensemble average number of days per month when daily maximum 8-hour average O_3 concentrations exceed 60 ppb resulting from simultaneous 20% reductions in anthropogenic NO_x, CO, and NMVOC emissions within the source regions (colored lines; red = NA; green = EU; dark blue = EA; light blue = SA), spatially averaged over each receptor region (panels). Also shown are the model ensemble average DAYS>60 in the base case SR1 simulation for each region (black lines; right axes as indicated by arrows). The change is estimated by first calculating the area-weighted spatial average value for DAYS>60 in each model simulation for a given region,and then taking the multi-model average of the differences in these spatially averaged DAYS>60 values (SR1-SR6). Hourly surface O_3 values are taken from the SR6 and SR1 simulations in 13 models: CAMCHEM, ECHAM5-HAMMOZ, EMEP, FRSGC/UCI, GEMAQ-v1p0, GEOS-Chem-v07, GMI, LMDz3-INCA1, LLNL-IMPACT, MOZARTGFDL, MOZECH, TM5-JRC-cy2-ipcc, UM-CAM.